nature neuroscience

# Neddylation inhibition impairs spine development, destabilizes synapses and deteriorates cognition

Annette M Vogl[1,11], Marisa M Brockmann[1,11], Sebastian A Giusti[1], Giuseppina Maccarrone[2], Claudia A Vercelli[3], Corinna A Bauder[1], Julia S Richter[1], Francesco Roselli[4,5,10], Anne-Sophie Hafner[6,7], Nina Dedic[4,8], Carsten T Wotjak[4], Daniela M Vogt-Weisenhorn[8], Daniel Choquet[6,7], Christoph W Turck[2], Valentin Stein[9], Jan M Deussing[4] & Damian Refojo[1]

**Neddylation is a ubiquitylation-like pathway that controls cell cycle and proliferation by covalently conjugating Nedd8 to specific targets. However, its role in neurons, nonreplicating postmitotic cells, remains unexplored. Here we report that Nedd8 conjugation increased during postnatal brain development and is active in mature synapses, where many proteins are neddylated. We show that neddylation controls spine development during neuronal maturation and spine stability in mature neurons. We found that neddylated PSD-95 was present in spines and that neddylation on Lys202 of PSD-95 is required for the proactive role of the scaffolding protein in spine maturation and synaptic transmission. Finally, we developed *Nae1*$^{CamKII\alpha\text{-}CreERT2}$ mice, in which neddylation is conditionally ablated in adult excitatory forebrain neurons. These mice showed synaptic loss, impaired neurotransmission and severe cognitive deficits. In summary, our results establish neddylation as an active post-translational modification in the synapse regulating the maturation, stability and function of dendritic spines.**





The very dynamic processes of synapse development and function are controlled by several post-translational modifications that fine-tune the interactions, trafficking, stability, localization and activity of proteins. In recent years, the importance of ubiquitylation and the ubiquitylation-like pathway sumoylation in different aspects of synapse development and plasticity has been well established[1,2]. In contrast, the role of other ubiquitin-like proteins (UBLs) remains largely unknown. The UBL family consists of a set of evolutionarily conserved polypeptides with high similarity to ubiquitin and of a similar three-dimensional structure that can be reversibly conjugated to target proteins through isopeptide bonds to lysine residues[3].

UBLs include, in decreasing order of sequence similarity to ubiquitin, Nedd8, Fub1, Isg15, Fat10, Hub1, Sumo1–3, Ufm1, Urm1 and the autophagy-related proteins Atg8 and Atg12 (ref. 3). With the exception of Sumo1–3, the role of UBLs in neuronal development in general and synaptic differentiation and plasticity in particular is almost unexplored. This is particularly surprising for Nedd8 (neural precursor cell–expressed developmentally downregulated gene 8), a UBL ~80% homologous to ubiquitin that was originally discovered in embryonic brain tissue and whose mRNA expression in the brain was described as developmentally downregulated[4].

Similar to ubiquitylation, neddylation requires three sequential reaction steps accomplished by the heterodimeric E1-activating enzyme NAE (Nedd8 activating enzyme), the conjugating enzyme Ubc12 and an as yet incompletely characterized set of E3 ligases[5]. The best-documented function of Nedd8 is to target cullin scaffold proteins, thereby increasing the activity of cullin-RING E3 ubiquitin-ligase complexes (CRLs), which are mainly involved in the control of cell cycle and cellular proliferation[6]. Recent reports indicate that neddylation also influences the enzymatic activity, transcriptional function, protein stability and partner interaction of several non-cullin substrates, suggesting additional functions of Nedd8 conjugation beyond CRLs[5,7]. The only relevant target for neuronal physiology or dysfunction described so far is the Parkinson-related protein Parkin; it has been recently reported that its ubiquitin E3-ligase activity increases upon neddylation[8]. Besides that, Nedd8 has been associated only with neurite differentiation in *Drosophila* as part of larger genetic screens[9].

We report here that neddylation increased during postnatal brain development, was active within mature synapses and regulated synaptogenesis during neuronal development. In mature neurons neddylation promoted spine stability and was required for the proactive function of the scaffolding protein PSD-95 in spine maturation and synaptic AMPA currents. Furthermore, ablation of the neddylation pathway in adult excitatory forebrain neurons in *Nae1* conditional knockout mice led to severe synaptic loss, impaired neurotransmission and cognitive deficits.

[1]Molecular Neurobiology, Max Planck Institute of Psychiatry, Munich, Germany. [2]Department for Translational Research in Psychiatry, Max Planck Institute of Psychiatry, Munich, Germany. [3]Instituto de Investigación en Biomedicina de Buenos Aires (IBioBA)-CONICET-Partner Institute of the Max Planck Society, Buenos Aires, Argentina. [4]Department of Neurobiology of Stress and Neurogenetics, Max Planck Institute of Psychiatry, Munich, Germany. [5]Department of Neuroscience, Section of Neurology, University of Bari, Bari, Italy. [6]University of Bordeaux, Interdisciplinary Institute for Neuroscience, Bordeaux, France. [7]CNRS UMR 5297, Bordeaux, France. [8]Institute of Developmental Genetics, Helmholtz-Zentrum München, Neuherberg, Germany. [9]Institute of Physiology, University of Bonn, Bonn, Germany. [10]Present address: Departments of Neurology and Anatomy, Ulm University School of Medicine, Ulm, Germany. [11]These authors contributed equally to this work. Correspondence should be addressed to D.R. (damian.refojo@gmail.com).

Received 4 October 2014; accepted 4 December 2014; published online 12 January 2015; doi:10.1038/nn.3912

## RESULTS

### Nedd8 is the most abundant UBL in neurons

To specifically determine the neuronal expression of various UBLs, we profiled the mRNA levels of *Sumo1–3*, *Ufm1*, *Urm1*, *Isg15*, *Fat10*, *Nedd8* and *Hub1* by quantitative real-time polymerase chain reaction (qRT-PCR) in embryonic neuronal cultures (**Fig. 1a**). We excluded the UBL Fub1 from the analysis because it is cotranscribed as a fusion mRNA with the ribosomal protein S30 (ref. 3), which might act as a confounding factor. *Nedd8* and *Hub1* mRNAs were the most abundant UBL mRNAs in both immature (**Supplementary Fig. 1a**) and fully mature neurons (**Fig. 1a**). Hub1 lacks the typical diglycine (di-Gly) C-terminal end and binds proteins in a noncovalent manner[3]. These results prompted us to study the role of neddylation in neurons.

So far a systematic mapping of the expression profile of Nedd8 in adult and developmental brains has not been done. Using *in situ* hybridization (ISH), we found that both *Nedd8* and *Ubc12* mRNAs were broadly expressed in neurons throughout embryonic and adult mouse brain (**Fig. 1b** and **Supplementary Fig. 1b–d**). To further corroborate these findings, we took advantage of a conventional *Ubc12* knockout mouse line that carries a β-galactosidase-based reporter in the targeting cassette (**Supplementary Fig. 1e**). Whereas homozygous null mice die at early embryonic stages, heterozygous *Ubc12* knockout mice do not present gross morphological or behavioral abnormalities (data not shown). LacZ staining of the brains of heterozygous mice showed ubiquitous Ubc12 expression, similar to the results obtained in ISH experiments (**Fig. 1c** and **Supplementary Fig. 1e**).

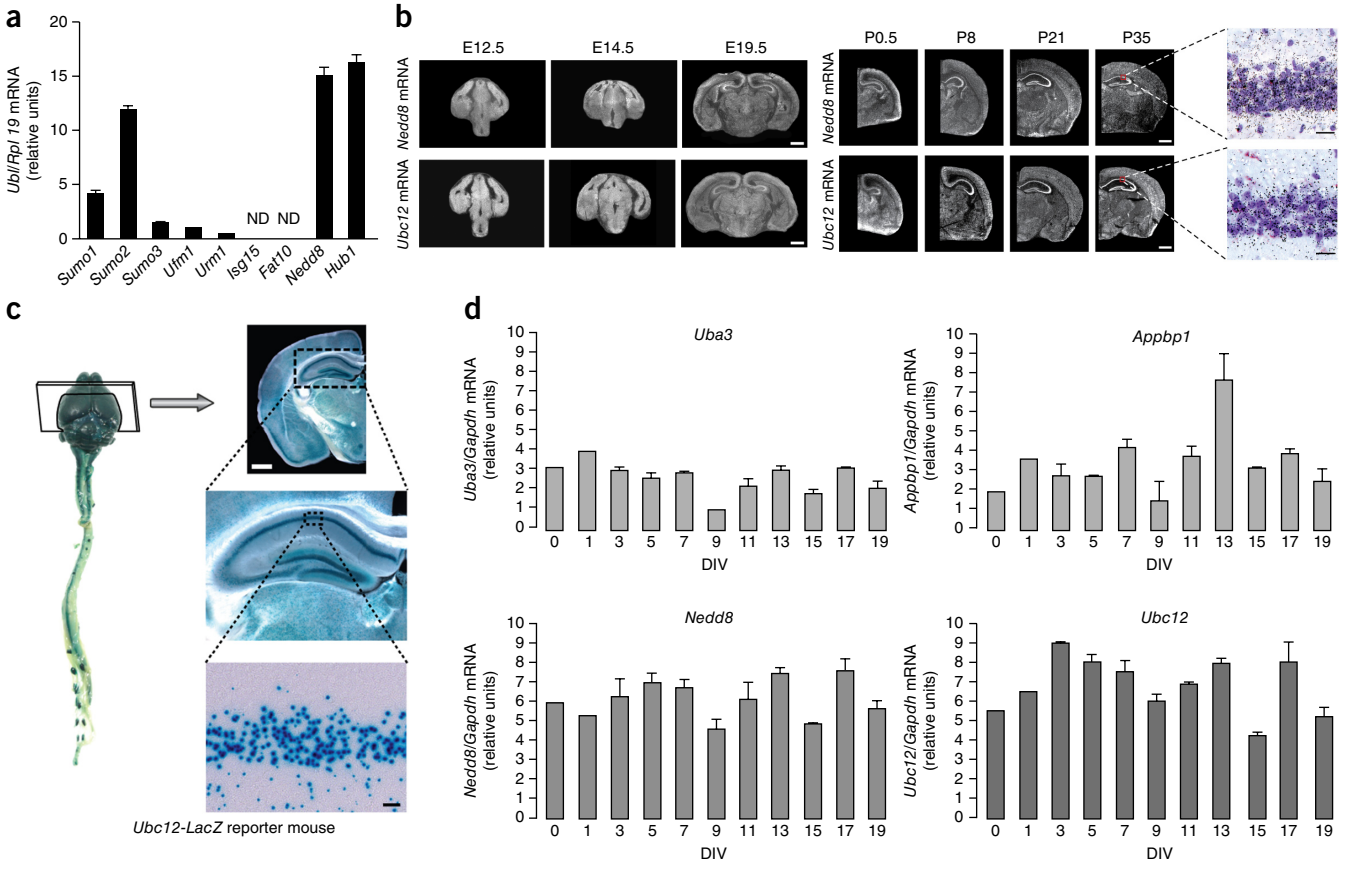


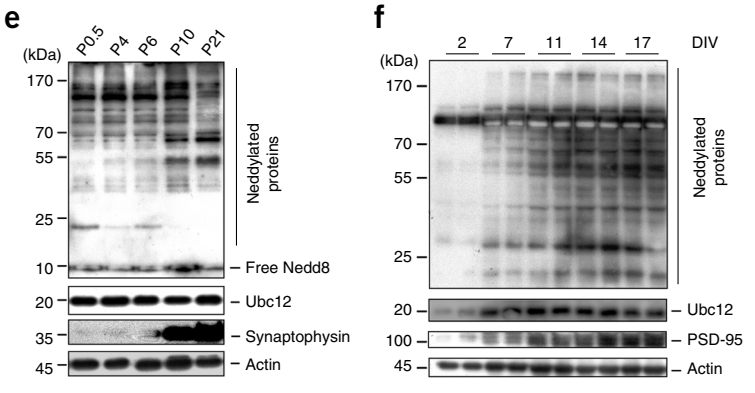


**Figure 1** Nedd8 is the most abundantly expressed UBL in neurons and is broadly expressed in the mouse brain. (**a**) Real-time qRT-PCR of *Ubl* mRNAs in DIV14 mouse cortical neurons, $n = 4$, from two cultures. ND, not detectable. (**b**) Left, dark-field photomicrographs of *Nedd8* and *Ubc12 in situ* hybridizations. Scale bars, 1 mm. Right, neuron-enriched mRNA expression of *Nedd8* and *Ubc12* (black dots) in hippocampal CA1 neurons (cresyl violet staining) in higher-magnification bright-field photomicrographs. Scale bars, 25 μm. (**c**) LacZ stainings of *Ubc12-LacZ* reporter mice. Scale bar, 1 mm (25 μm in the bottom panel). (**d**) No changes in real-time qRT-PCR analysis of *Uba3*, *Appbp1*, *Nedd8* and *Ubc12* mRNA expression during development of rat hippocampal neurons, $n = 3$, from three cultures. DIV, days *in vitro*. (**e**,**f**) Nedd8 conjugation increased during brain and neuronal development. Immunoblotting of lysates from total mouse brain (**e**) and mouse hippocampal neurons (**f**). Data are presented as mean ± s.e.m. Images in **b**, **c**, **e** and **f** represent data from at least two experiments. Full-length blots are presented in **Supplementary Figure 10**.

### Neddylated substrates increase with neuronal development

Nedd8 was originally identified from northern blotting experiments showing that it was downregulated during brain development[4]. In contrast, ISH did not reveal significant changes in *Nedd8* expression during brain development in our study, in either embryonic or early postnatal brains (**Fig. 1b**). As assessed by qRT-PCR, the levels of the mRNAs encoding both E1-NAE subunits (*Uba3* and *Nae1* (also known as *Appbp1*)), the E2 *Ubc12* and *Nedd8* did not change during neuronal development (**Fig. 1d**). The mRNA expression profiles of all cullin genes showed similar results (data not shown). Next we asked whether the protein levels of Nedd8 and Ubc12 or the patterns of neddylated proteins might change during development. We observed an increase of neddylated substrates in brain lysates (**Fig. 1e**) and primary neurons (**Fig. 1f**) during maturation. The differences in the pattern of neddylated proteins are probably due to the different sources of the samples probed (brain extracts versus purified neurons) (**Fig. 1e**,**f**).

Unfortunately, the sensitivity of the different Ubc12 and Nedd8 antibodies tested did not allow for reliable intracellular protein localization. A recent screening demonstrated that immunofluorescence of endogenous proteins and the transfection of constructs encoding fluorescent fusion variants led to the same subcellular distribution for most of the analyzed proteins[10]. Nedd8 and Ubc12, tagged with either Venus or hemagglutinin, localized to the soma, dendrites and dendritic spines in transfected mature hippocampal neurons (**Supplementary Fig. 1f**).

### Neddylation is necessary for dendritic spine maturation

As neddylation of neuronal proteins increases during postnatal brain development, we asked whether neddylation influences spine formation. We downregulated the Nedd8 pathway in young primary neurons at stages when filopodia start to emerge through the expression of shRNAs against Nedd8 or Ubc12 (**Supplementary Fig. 2a**,**b**), overexpression of a dominant negative Ubc12 (Ubc12-C111S) that sequesters Nedd8 (ref. 11) or treatment with the well-established NAE inhibitor MLN-4924 (ref. 7) (**Supplementary Fig. 2c**). All three approaches prevented the development of mature mushroom-like spines, resulting in dendrites decorated with filopodia, which were

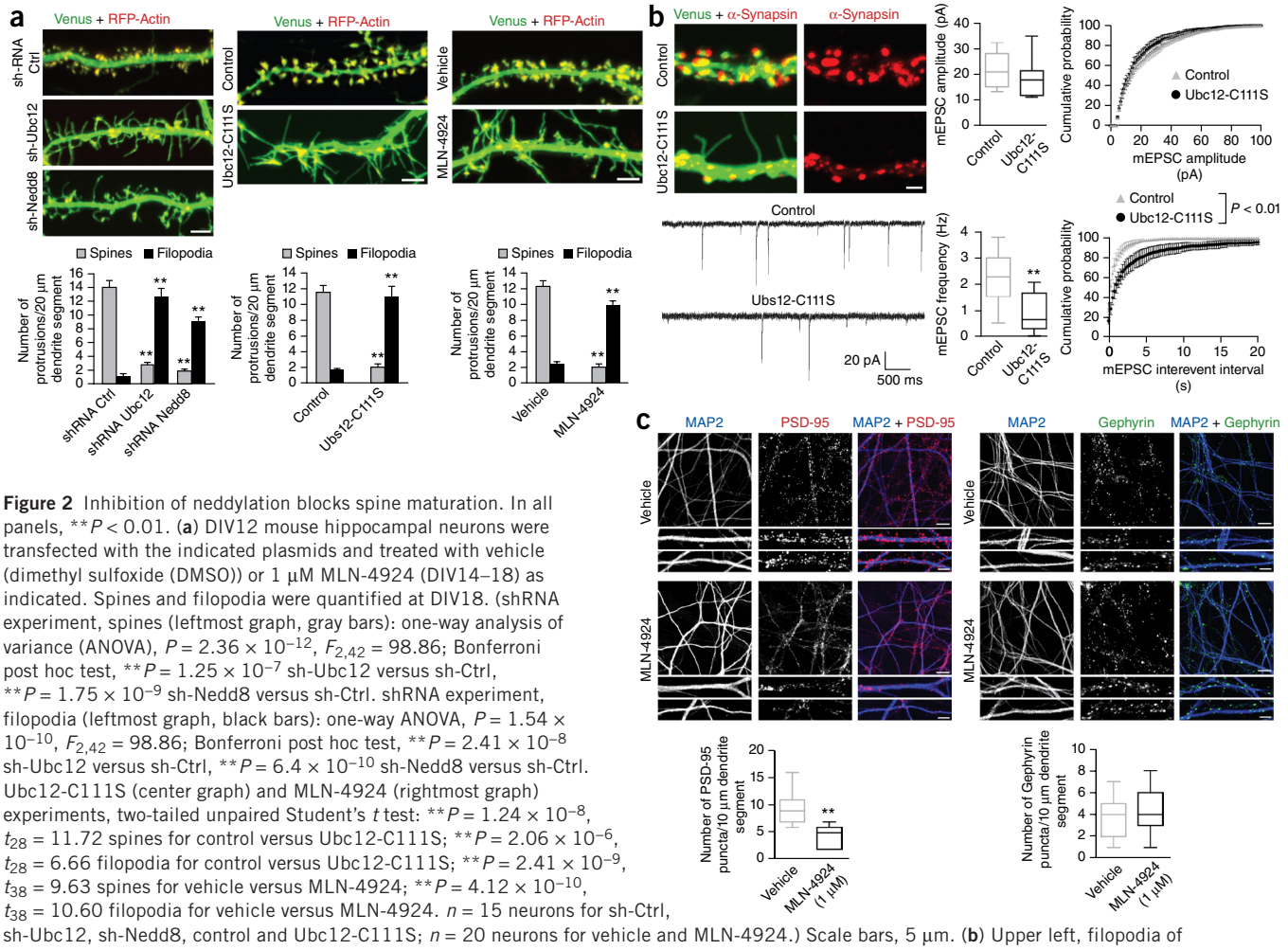


**Figure 2** Inhibition of neddylation blocks spine maturation. In all panels, $^{**}P < 0.01$. (**a**) DIV12 mouse hippocampal neurons were transfected with the indicated plasmids and treated with vehicle (dimethyl sulfoxide (DMSO)) or 1 µM MLN-4924 (DIV14–18) as indicated. Spines and filopodia were quantified at DIV18. (shRNA experiment, spines (leftmost graph, gray bars): one-way analysis of variance (ANOVA), $P = 2.36 \times 10^{-12}$, $F_{2,42} = 98.86$; Bonferroni post hoc test, $^{**}P = 1.25 \times 10^{-7}$ sh-Ubc12 versus sh-Ctrl, $^{**}P = 1.75 \times 10^{-9}$ sh-Nedd8 versus sh-Ctrl. shRNA experiment, filopodia (leftmost graph, black bars): one-way ANOVA, $P = 1.54 \times 10^{-10}$, $F_{2,42} = 98.86$; Bonferroni post hoc test, $^{**}P = 2.41 \times 10^{-8}$ sh-Ubc12 versus sh-Ctrl, $^{**}P = 6.4 \times 10^{-10}$ sh-Nedd8 versus sh-Ctrl. Ubc12-C111S (center graph) and MLN-4924 (rightmost graph) experiments, two-tailed unpaired Student's *t* test: $^{**}P = 1.24 \times 10^{-8}$, $t_{28} = 11.72$ spines for control versus Ubc12-C111S; $^{**}P = 2.06 \times 10^{-6}$, $t_{28} = 6.66$ filopodia for control versus Ubc12-C111S; $^{**}P = 2.41 \times 10^{-9}$, $t_{38} = 9.63$ spines for vehicle versus MLN-4924; $^{**}P = 4.12 \times 10^{-10}$, $t_{38} = 10.60$ filopodia for vehicle versus MLN-4924. $n = 15$ neurons for sh-Ctrl, sh-Ubc12, sh-Nedd8, control and Ubc12-C111S; $n = 20$ neurons for vehicle and MLN-4924.) Scale bars, 5 µm. (**b**) Upper left, filopodia of neddylation-deficient neurons do not establish synaptic contacts. Mouse hippocampal neurons, transfected at DIV12, were immunostained for Synapsin at DIV18. Scale bar, 2.5 µm. Upper and lower right, decreased mEPSC frequency and preserved mEPSC amplitude in Ubc12-C111S-expressing neurons. mEPSCs of transfected (DIV12) mouse hippocampal neurons were recorded at DIV16–18; mean values are shown on the left, and distributions on the right (Kolmogorov-Smirnov test, $^{**}P < 0.01$; $n = 10$ control neurons, 11 Ubc12-C111S neurons). Lower left, representative sample traces of mEPSCs. (**c**) Neddylation controls the development of excitatory synapses. The number of excitatory, PSD-95-labeled (left), and inhibitory Gephyrin-labeled (right) puncta was analyzed in mouse hippocampal neurons treated with vehicle or 1 µM MLN-4924 at DIV13 for 48 h (two-tailed unpaired Student's *t* test: PSD-95, $^{**}P < 7.38 \times 10^{-6}$, $t_{28} = 5.49$; Gephyrin, $P = 0.75$, $t_{28} = 0.31$; $n = 15$ fields). Scale bars, 10 µm (5 µm in lower images). Data are presented as mean ± s.e.m. and box-and-whisker plots (box limits represent first and third quartiles, center line represents median, and whiskers represent minimum and maximum values). Images and quantifications represent data from three experiments.

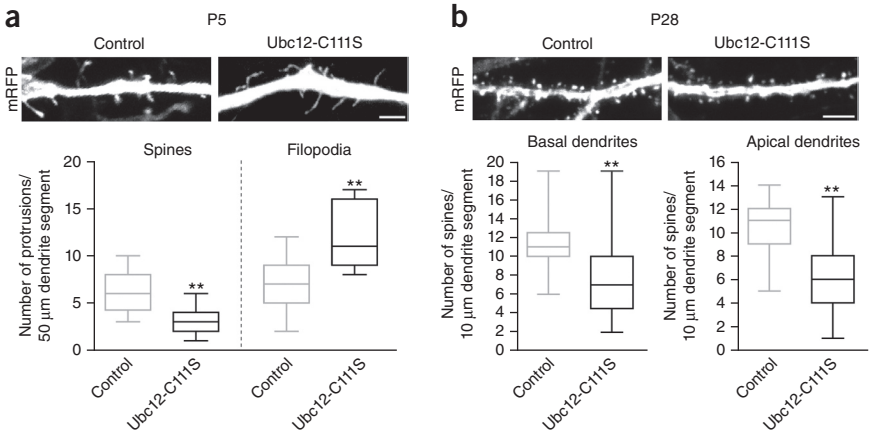


**Figure 3** Neddylation regulates spine maturation *in vivo*. In all panels, $^{**}P < 0.01$. (**a**,**b**) Mouse hippocampal CA1 pyramidal neurons were *in utero* electroporated at E14.5 with mRFP and control or Ubc12-C111S plasmids. Inhibition of neddylation decreased the number of spines and increased the number of filopodia at P5 (**a**) and P28 (**b**) (two-tailed unpaired Student's *t* test: $^{**}P = 0.0002$ for spines and filopodia, $t_{28} = 4.53$ for spines, $t_{28} = 4.27$ for filopodia (**a**); $^{**}P = 0.0013$, $t_{28} = 3.56$ for basal dendrites; $^{**}P = 2.02 \times 10^{-7}$, $t_{28} = 6.29$ for apical dendrites (**b**); $n = 14$ control neurons or 16 Ubc12-C111S neurons from four brains). Scale bars, 5 µm. Data are presented as box-and-whisker plots (box limits represent first and third quartiles, center line represents median, and whiskers represent minimum and maximum values). Images and quantifications represent data from two experiments.

shown to be spine precursors[12–14] (**Fig. 2a**). Potential off-target effects of the shRNAs against Nedd8 or Ubc12 were ruled out by reversion experiments with shRNA-resistant versions of Ubc12 and Nedd8 (**Supplementary Fig. 2d**). This indicates that spine development requires neddylation. Functional downregulation of every single cullin with dominant-negative constructs or inhibition of all cullins in unison with RBX1 dominant-negative or shRNAi constructs did not recapitulate the phenotype observed after the inhibition of neddylation (**Supplementary Fig. 2e–g**). This suggests that additional targets aside from CRLs mediate the effects of neddylation on spine development.

Transient synaptic contacts of filopodia with presynaptic boutons have been reported in several studies[12,13,15]. In contrast, filopodia of Ubc12-C111S-expressing neurons did not establish synaptic contacts in the current study (**Fig. 2b**). Upon neddylation blockade, a profound decrease in synapses on spines was accompanied by a parallel increase in synapses on dendritic shafts, although this was not sufficient to restore the normal total number of synapses (**Fig. 2c** and **Supplementary Fig. 2h**). Indeed, Ubc12-C111S-expressing neurons showed a significant reduction in miniature excitatory postsynaptic current (mEPSC) frequency (**Fig. 2b**), reflecting the reduced number of synapses. The amplitude of mEPSCs was not affected (**Fig. 2b**), suggesting that the remaining synapses on the shaft were functionally intact. Furthermore, MLN-4924 reduced the number of PSD-95 puncta but did not affect the density of GABAergic synapses, indicating that neddylation specifically influences excitatory synapse formation (**Fig. 2c**).

To further confirm the effects of neddylation *in vivo*, we expressed Ubc12-C111S in hippocampal neural progenitors by means of *in utero* electroporation (IUE). Expression of Ubc12-C111S during neuronal development increased the number of filopodia in pyramidal neurons at P5 (**Fig. 3a**), resulting in a reduced spine density at P28 (**Fig. 3b**). Taken together, these results demonstrate that neddylation is critical for dendritic spine development in primary neurons and *in vivo*.

Reduced filopodia motility might account for the impaired synapse development[12,13,15]. Live imaging experiments clearly indicated that the filopodia of neddylation-deficient neurons are dynamic (**Supplementary Fig. 3a,b**), suggesting that neddylation might affect the stabilization of filopodia rather than their motility, two processes that are differentially regulated in developing pyramidal neurons[15].

## Neddylation is active in spines and controls their stability

Structural stabilization of spines is not only necessary during late spine development but also instrumental in the maintenance of mature spines[16–18]. This implies that neddylated proteins should be present in spines. In fact, we probed synaptosomal fractions and found Ubc12 as well as many neddylated proteins differentially expressed in pre- and postsynaptic compartments (**Fig. 4a**). Further purifications of postsynaptic membranes indicated that the Triton-soluble and -insoluble fractions of the postsynaptic density contained different sets of neddylated proteins (**Fig. 4a**). To our knowledge these results represent the first description of neddylation as an active post-translational modification of synaptic proteins.

Next, we asked whether neddylation affects mature spines. We applied IUE to embryos from *CamKIIα*$^{CreERT2}$ × *CD1* breedings with a floxed-stop Ubc12-C111S-IRES-GFP plasmid and prepared mixed (*CamKIIα*$^{CreERT2}$-positive and -negative) dissociated neuronal cultures at E17.5 (**Supplementary Fig. 3c**). Later, we induced the expression of Ubc12-C111S with 4-OH-tamoxifen at DIV17. Since spine density stabilizes around DIV15 (**Supplementary Fig. 3d**), this method allows genetic manipulations in mixed cultures of fully mature neurons (DIV17–20) without transfections that may compromise neuronal function or survival at those mature stages *in vitro*. Ubc12-C111S expression led to reduced spine density (**Supplementary Fig. 3e**), suggesting that neddylation inhibition destabilizes spines.

To further test this hypothesis, we performed live imaging experiments and quantified the rates of *de novo* growth and elimination of spines in mature cultured neurons (DIV19) treated for 8 h with vehicle or MLN-4924 (**Fig. 4b**). Whereas only 10.1% ± 2% were lost in control conditions, 49.8% ± 3% of the spines were lost after 8 h of MLN-4924 treatment. In contrast, the percentage of newly formed spines did not significantly differ between groups (**Fig. 4b**).

Next we analyzed changes of spine morphology after transient MLN-4924 treatment. The inhibitor caused significant shrinkage of mature spines 150 min after application, and 57.1% of spines (here called Nedd8-responsive type I) recovered within 2 h after MLN-4924 washout (**Fig. 4c–e**). However, a distinct population of shrunk spines (34.3%; Nedd8-responsive type II) did not recover to their original size, and 8.6% of the spines remained resistant to MLN-4924 treatment (Nedd8-responsive type III) (**Fig. 4c–e**). This indicates that individual spines from the same neuron do not respond to changes in neddylation homogeneously. The capability of spines to recover from neddylation inhibition was independent of initial spine size (Pearson's test, $r = -0.1824$, $P = 0.309$).

To further corroborate the role of neddylation in spine elimination *in vivo*, we transfected hippocampal progenitors of *CamKIIα*$^{CreERT2}$ and wild-type (WT) littermate mice by IUE with an inducible

CAG-floxed STOP-Ubc12-C111S plasmid together with CAG-mRFP as a volume marker and CAG-floxed STOP-EGFP to report inducibility and control leakiness (**Fig. 5** and **Supplementary Fig. 4a**). At P35, when pyramidal neurons were fully matured, Ubc12-C111S expression was switched on by tamoxifen administration. In line with our previous results, dentate granule neurons and CA1 pyramidal (**Fig. 5**) and cortical neurons (**Supplementary Fig. 4b**) of *CamKIIα*$^{CreERT2}$ mice displayed a significant reduction in spine density relative to WT littermates.

Taken together, these data suggest that neddylation is a key factor for spine maintenance in principal neurons.

## Neddylation targets the scaffolding protein PSD-95

Which potential Nedd8 targets might contribute to the main effects of neddylation in the spine?

It is probably unrealistic to expect that neddylation of a single protein explains the effects triggered by the entire Nedd8 pathway. However, the question is relevant, in general because nonclassical post-translational modifications of synaptic proteins are understudied[19], and in particular for neddylation, as no synaptic targets have been described so far. Scaffolding proteins are attractive candidates because they structurally and functionally organize the postsynaptic density in both immature and mature spines[18]. We tested the

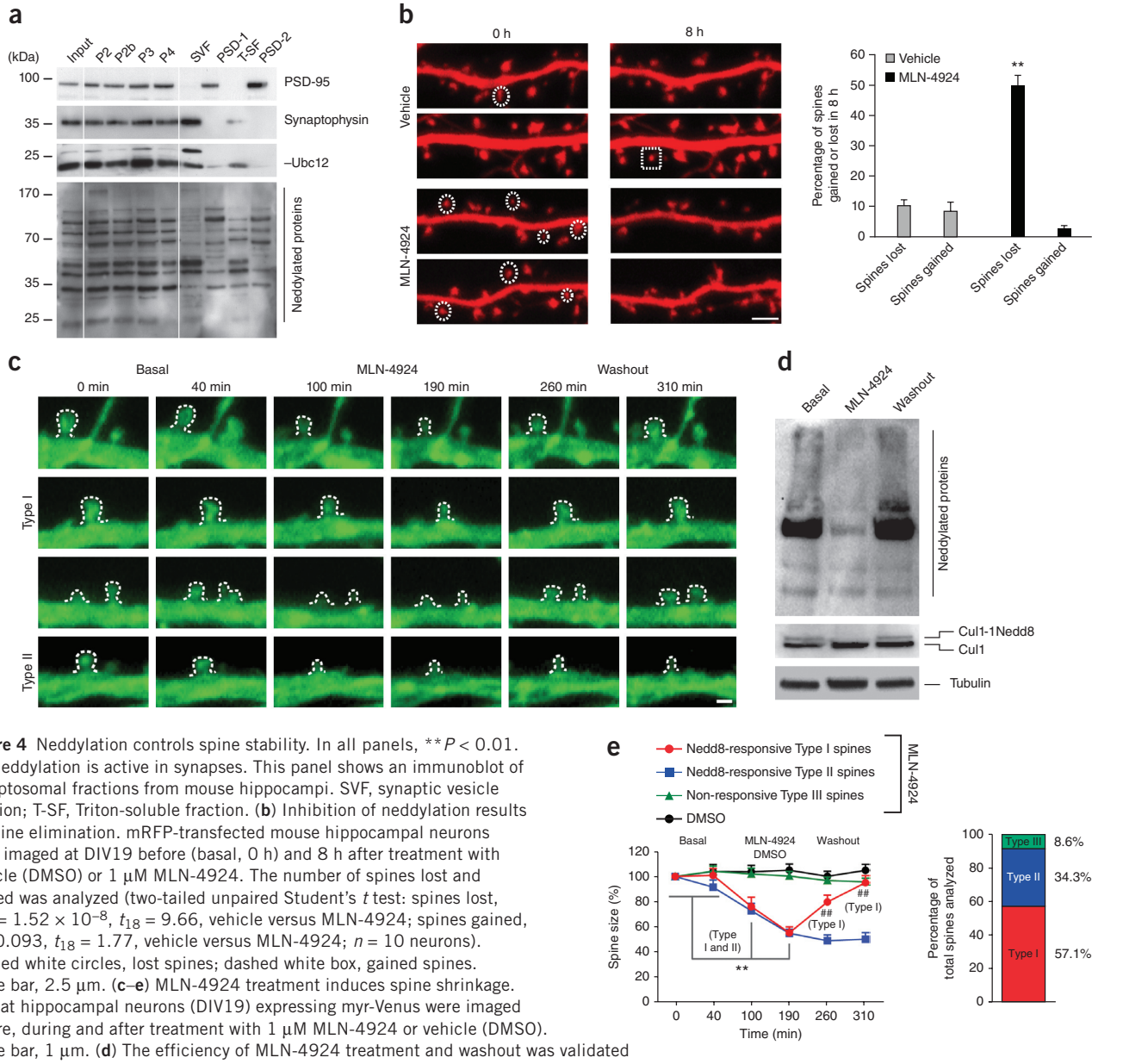


**Figure 4** Neddylation controls spine stability. In all panels, $^{**}P < 0.01$. (**a**) Neddylation is active in synapses. This panel shows an immunoblot of synaptosomal fractions from mouse hippocampi. SVF, synaptic vesicle fraction; T-SF, Triton-soluble fraction. (**b**) Inhibition of neddylation results in spine elimination. mRFP-transfected mouse hippocampal neurons were imaged at DIV19 before (basal, 0 h) and 8 h after treatment with vehicle (DMSO) or 1 μM MLN-4924. The number of spines lost and gained was analyzed (two-tailed unpaired Student's *t* test: spines lost, $^{**}P = 1.52 \times 10^{-8}$, $t_{18} = 9.66$, vehicle versus MLN-4924; spines gained, $P = 0.093$, $t_{18} = 1.77$, vehicle versus MLN-4924; $n = 10$ neurons). Dashed white circles, lost spines; dashed white box, gained spines. Scale bar, 2.5 μm. (**c**–**e**) MLN-4924 treatment induces spine shrinkage. (**c**) Rat hippocampal neurons (DIV19) expressing myr-Venus were imaged before, during and after treatment with 1 μM MLN-4924 or vehicle (DMSO). Scale bar, 1 μm. (**d**) The efficiency of MLN-4924 treatment and washout was validated by immunoblotting. (**e**) Spine size was measured. (One-way ANOVA repeated measures: red curve, $P = 0.0001$, $F_{5,45} = 12.46$; blue curve, $P = 0.0001$, $F_{5,45} = 33.11$; green curve, $P = 0.068$, $F_{5,45} = 2.29$; black curve, $P = 0.884$, $F_{5,45} = 0.34$. Bonferroni post hoc test: red curve, $^{**}P = 0.0093$ for 0 versus 100 min, $^{**}P = 1.53 \times 10^{-6}$ for 0 versus 190 min, $^{**}P = 0.005$ for 40 versus 100 min, $^{**}P = 0.00021$ for 40 versus 190 min, $^{\#\#}P = 4.97 \times 10^{-5}$ for 190 versus 260 min, $^{\#\#}P = 2.28 \times 10^{-5}$ for 190 versus 310 min; blue curve, $^{**}P = 0.0011$ for 0 versus 100 min, $^{**}P = 1.64 \times 10^{-7}$ for 0 versus 190 min, $^{**}P = 0.009$ for 40 versus 100 min, $^{**}P = 6.95 \times 10^{-5}$ for 40 versus 190 min; $n = 10$ neurons.) Spines were grouped as Type I (reversible: decrease during MLN-4924 treatment + recovery after MLN-4924 washout), Type II (irreversible: no recovery after MLN-4924 washout) or Type III (nonresponsive spines). Data are presented as mean ± s.e.m. Images and quantifications in **a** and **c**–**e** represent data from three experiments. Images and quantifications in **b** represent data from two experiments. Full-length blots are presented in **Supplementary Figure 10**.

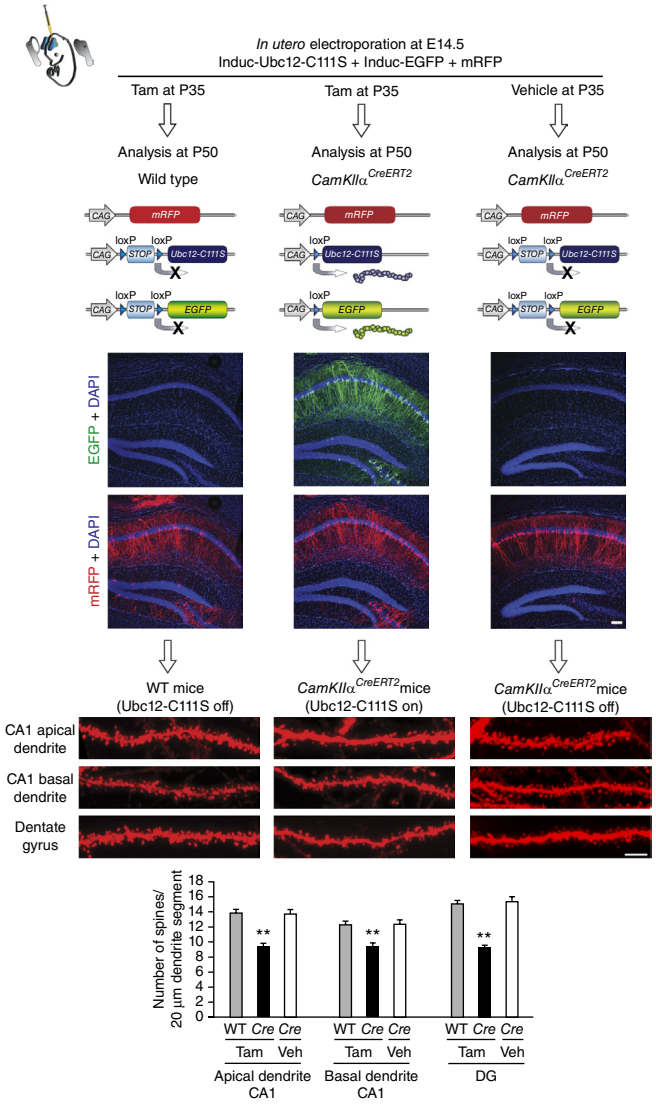


**Figure 5** Ubc12-C111S impairs spine maintenance *in vivo*. Pyramidal hippocampal neurons in CA1 and granule neurons of the dentate gyrus (DG) were *in utero* electroporated at E14.5 with inducible Ubc12-C111S, inducible EGFP and constitutive mRFP plasmids in WT and *CamKIIα*$^{CreERT2}$ mouse embryos. At P35 tamoxifen (Tam) or vehicle (Veh) was applied, and at P50 spine number was analyzed. (One-way ANOVA: CA1 apical, $P = 1.28 \times 10^{-7}$, $F_{2,39} = 24.50$; CA1 basal, $P = 0.0002$, $F_{2,39} = 10.77$; DG, $P = 1.52 \times 10^{-11}$, $F_{2,39} = 50.46$. Bonferroni post hoc test: CA1 apical, $^{**}P = 3.68 \times 10^{-7}$; CA1 basal, $^{**}P = 0.00024$; DG, $^{**}P = 3.8 \times 10^{-11}$. All for *Cre* Tam versus WT Tam; $n = 14$ neurons from six brains.) Scale bars, 100 µm (top) and 5 µm (bottom). Data are presented as mean ± s.e.m. Images and quantifications represent data from three experiments. DAPI, 4,6-diamidino-2-phenylindole. $^{**}P < 0.01$.

neddylation of MAGUK, Homer, GKAP and Shank proteins in neurons by purifying Nedd8 fused to a biotinylatable tag (Biotin-Nedd8) under denaturing conditions (**Supplementary Fig. 5a–d**). Only PSD-95 was found neddylated, and this modification was prevented by MLN-4924 treatment (**Fig. 6a**). This effect was corroborated in heterologous HEK293 cells under both nondenaturing and denaturing conditions (**Supplementary Fig. 5e–g**). These results prompted us to investigate the neddylation of endogenous PSD-95 in more detail.

Next, we tried to detect the shift in molecular weight of endogenous neddylated PSD-95 after immunoprecipitation. Unfortunately, the low abundance of neddylated PSD-95 prevented the direct detection of a shifted band. To overcome this problem, we cut the blotted membrane to separate the lower band (abundant unconjugated PSD-95) from the upper band (neddylated PSD-95). This approach allowed us to improve sensitivity by increasing antibody concentration and exposure times. Thus, we were able to detect endogenously neddylated PSD-95 from primary neurons after immunoprecipitation and immunoblotting with both anti-PSD-95 and anti-Nedd8 antibodies. In both cases the positive shifted bands were strongly reduced in MLN-4924-treated samples (**Fig. 6b**). Similar results were obtained when we used purified synaptosomes as the starting material, further demonstrating that PSD-95 from synaptic sources is neddylated (**Supplementary Fig. 6a**).

Nedd8 bound to cullins is removed by the COP9 signalosome, whereas studies in *Drosophila* suggest that non-cullin neddylated proteins are deneddylated by Nedp1 (also known as DEN1 and Senp8)[20]. Hence, we generated *Nedp1*$^{-/-}$ mice and analyzed the neddylation of PSD-95 from cultured neurons obtained from these mice. Levels of neddylated PSD-95 were considerably higher in neurons from *Nedp1*$^{-/-}$ mice than in those from *Nedp1*$^{+/+}$ mice (**Fig. 6c**). The presence of endogenous PSD-95 in the shifted Nedd8–PSD-95 bands was independently confirmed by mass spectrometry (see gray arrowheads in **Fig. 6b,c** and **Supplementary Fig. 6a**). Similar to PSD-95 ubiquitylation[21], neddylation depends on the PEST domain of PSD-95 (**Fig. 6d**), which is also necessary for the co-immunoprecipitation of PSD-95 and Ubc12 (**Fig. 6e,f**). Ubiquitylation of PSD-95 is mediated by Mdm2 (refs. 21,22), an E3 ligase that also mediates neddylation of p53 (ref. 5). PSD-95 neddylation was also blocked

**Figure 6** Molecular characterization of PSD-95 neddylation. (**a**) Screening of postsynaptic scaffolding proteins in neurons revealed PSD-95 as a target of Nedd8. Extracts from mouse cortical neurons, nucleofected with 6xHis-BIO-Nedd8 and PSD-95-GFP constructs and treated with vehicle (DMSO) or 1 µM MLN-4924 for 6 h at DIV18, were purified under denaturing conditions and analyzed by immunoblotting. WB, western blot. (**b**,**c**) Neddylation of endogenous PSD-95 was blocked by MLN-4924 and increased in *Nedp1*$^{-/-}$ neurons. Extracts from DIV18 mouse neurons treated with DMSO or 1 µM MLN-4924 for 6 h (**b**) or from *Nedp1*$^{+/+}$ and *Nedp1*$^{-/-}$ mice (**c**) were immunoprecipitated and analyzed by immunoblotting. The presence of PSD-95 in the upper shifted bands was corroborated by mass spectrometry (gray arrowheads). IP, immunoprecipitation; conc., concentration. (**d**) Neddylation of PSD-95 depends on its N-terminal PEST domain and is blocked by Ubc12-C111S. Extracts from transiently transfected HEK293 cells were immunoprecipitated and analyzed by immunoblotting. mut, mutated. (**e**) Co-immunoprecipitation of Ubc12 and PSD-95 depends on the N-terminal PEST domain of the scaffold in HEK293 cells. (**f**) Endogenous Ubc12 and PSD-95 co-immunoprecipitated in extracts of mature (DIV18) mouse cortical neurons. (**g**) The E3 ligase Mdm2 dominant-negative variant (C464A) decreased PSD-95 neddylation in HEK293 cells. (**h**,**i**) The maintenance of PSD-95 clusters within spines requires Nedd8 conjugation. (**h**) We observed decreased synaptic PSD-95 puncta intensity in MLN-4924-treated DIV21 mouse hippocampal neurons (one-way ANOVA, $P = 0.0025$, $F_{3,53} = 5.42$; Bonferroni post hoc test, $^{**}P = 0.0095$ for 0 min versus 1 h, $^{**}P = 0.0017$ for 0 min versus 2 h; $n = 12$ fields for time point 0; $n = 15$ fields for 30 min, 1 h and 2 h). Scale bar, 5 µm. (**i**) Reduced PSD-95 within postsynaptic density complexes of MLN-4924-treated (6 h) DIV18 mouse cortical neurons, analyzed by immunoprecipitation with α-pan-GKAP antibodies and immunoblotting (two-tailed unpaired Student's *t* test, $^{*}P = 0.016$, $t_4 = 3.98$; $n = 3$). Arrowheads indicate specific neddylated PSD-95 bands. The additional bands around 100 kDa represent neddylated coprecipitating proteins associated with PSD-95. Data are presented as mean ± s.e.m. Images and quantifications represent data from three experiments. Full-length blots are presented in **Supplementary Figure 10**. $^{**}P < 0.01$.

by the dominant-negative RING mutant Mdm2-C464A (**Fig. 6g**), suggesting that Mdm2 is the main ligase neddylating PSD-95. Note that when immunoprecipitations under nondenaturing conditions were employed, an additional neddylated band was observed at ~100 kDa (**Fig. 6d**,**g** and **Supplementary Figs. 5e** and **6a**). These bands were too small to correspond to Nedd8–PSD-95 and plausibly represent neddylated coprecipitating proteins, as previously described for ubiquitylated PSD-95 (ref. 21).

What might be the role of neddylation on PSD-95? The main function of PSD-95 is to spatially organize postsynaptic molecules[23–25]. Treatment of mature neurons with MLN-4924 reduced synaptic PSD-95 puncta intensity and resulted in a spread PSD-95 signal in the dendritic

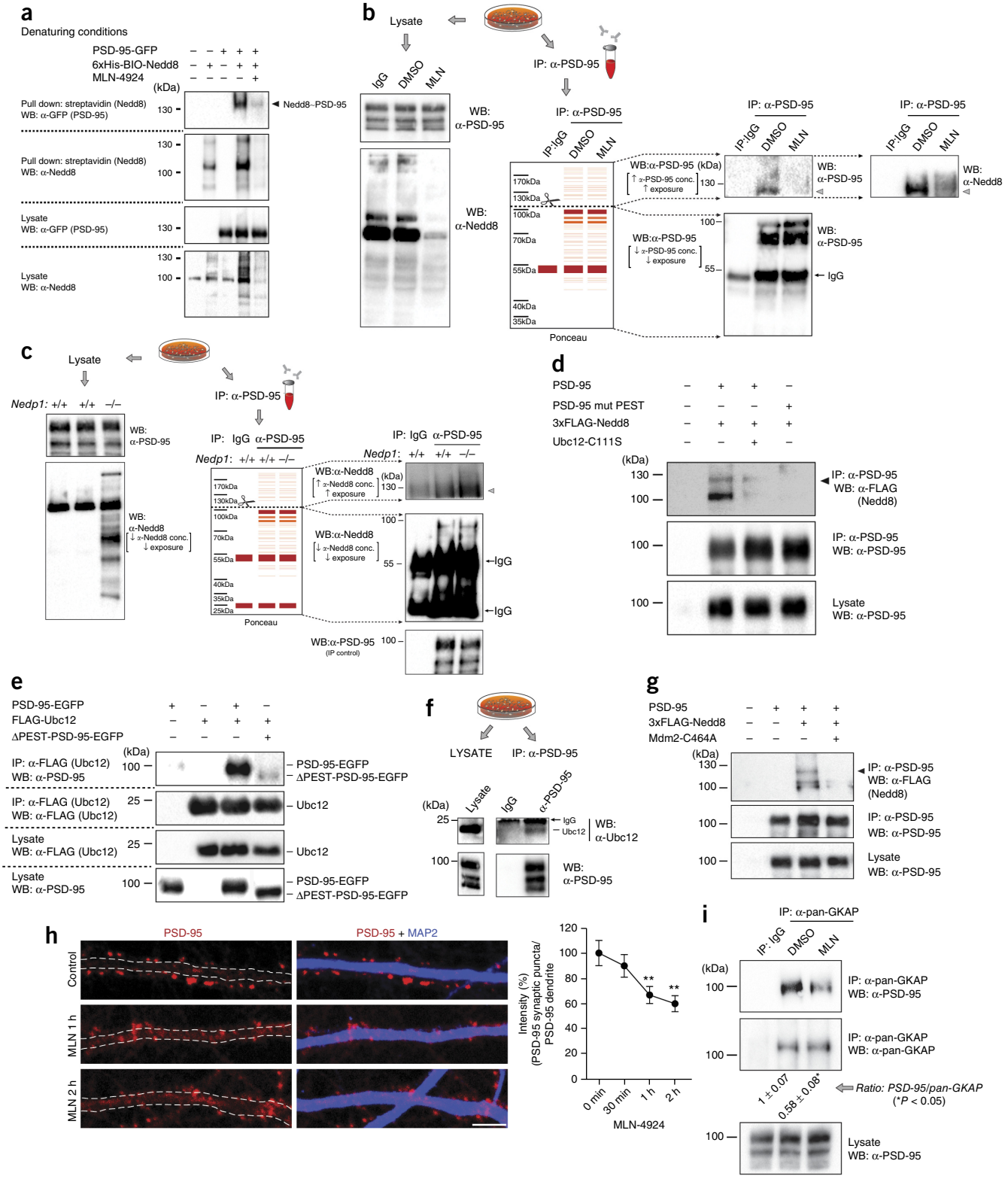

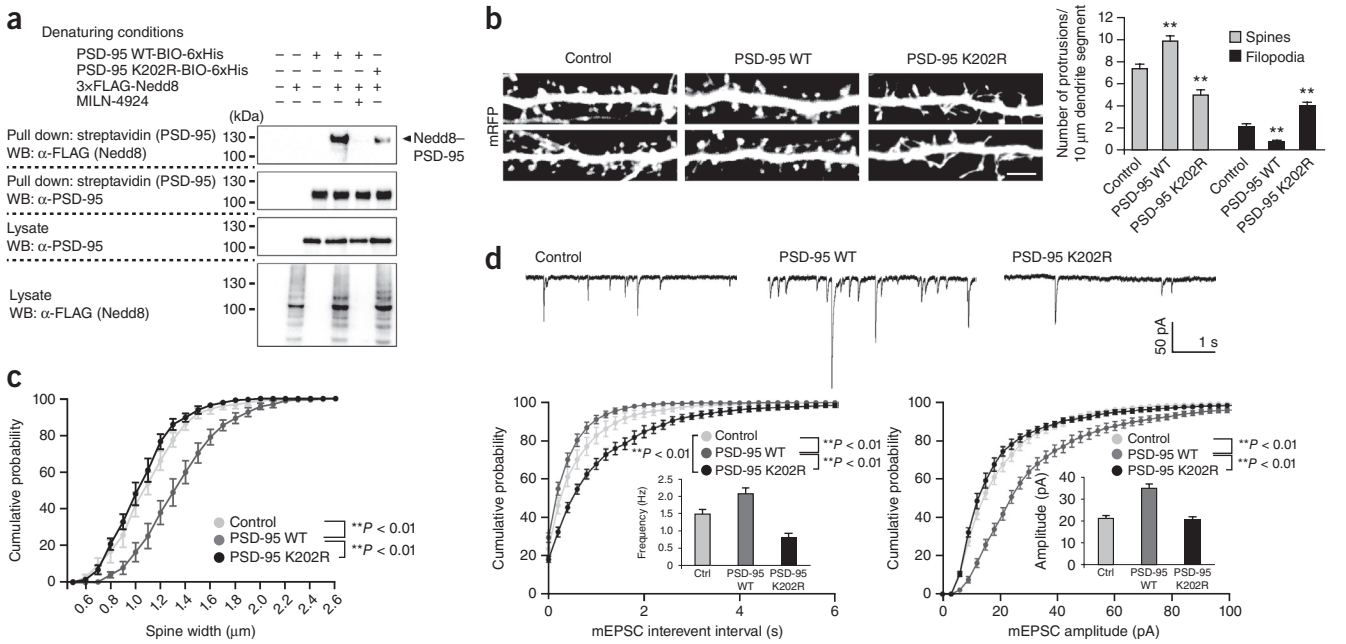


**Figure 7** Neddylation of Lys202 is required for the proactive role of PSD-95 in spine maturation and mEPSCs. (**a**) PSD-95 K202R showed reduced neddylation under denaturing conditions. Pulldown and immunoblotting of extracts from transiently transfected HEK293 cells treated with vehicle (DMSO) or 1 µM MLN-4924. (**b**) PSD-95 K202R impaired spine maturation. The number of spines and filopodia of transfected (DIV12–14) mouse hippocampal neurons was analyzed at DIV18–19. (One-way ANOVA: spines, $P = 4.82 \times 10^{-8}$, $F_{2,47} = 28.01$; filopodia, $P = 1.05 \times 10^{-12}$, $F_{2,47} = 43.56$. Bonferroni post hoc test: spines, $^{**}P = 0.0006$ for control versus PSD-95 WT, $^{**}P = 0.00084$ for control versus PSD-95 K202R; filopodia, $^{**}P = 4.59 \times 10^{-5}$ for control versus PSD-95 WT, $^{**}P = 3.34 \times 10^{-5}$ for control versus PSD-95 K202R. $n = 15$ neurons for control and PSD-95 WT, $n = 20$ neurons for PSD-95 K202R.) Scale bar, 5 µm. $^{**}P < 0.01$. (**c**) PSD-95 K202R failed to increase spine size. Spine width analyzed at DIV19 in transfected (DIV16) mouse hippocampal neurons (Kolmogorov-Smirnov test, $^{**}P < 0.01$; $n = 15$ neurons for control and PSD-95 WT, $n = 20$ neurons for PSD-95 K202R). (**d**) PSD-95 K202R reduced mEPSC frequency but did not alter mEPSC amplitude. Mouse organotypic hippocampal slice cultures were infected with Semliki Forest virus at DIV7–8, and mEPSCs were recorded at DIV9–10 (Kolmogorov-Smirnov test, $^{**}P < 0.01$; $n = 9$ neurons for control, 10 neurons for PSD-95 WT, and 8 neurons for PSD-95 K202R). Representative sample traces are shown. Data are presented as mean ± s.e.m. Images and quantifications represent data from three experiments. Full-length blots are presented in **Supplementary Figure 10**.

shaft (**Fig. 6h**), suggesting declustering and diffusion of the protein out of the spine. Accordingly, MLN-4924 also decreased the content of the scaffolding molecule in immunopurified postsynaptic density complexes (**Fig. 6i**).

Proteasome-mediated degradation of PSD-95 is induced by different treatments in neurons[21,22,26,27]. Although neddylation can either favor or inhibit the degradation of target proteins[3,5], MLN-4924 treatment did not alter PSD-95 protein levels in neuronal extracts or synaptodendritic-enriched fractions (**Supplementary Fig. 6b**,**c**). Furthermore, PSD-95 degradation rates remained unaffected in the presence of MLN-4924 (**Supplementary Fig. 6d**).

Taken together, these results indicate that neddylation controls the clustering function of PSD-95 but does not affect its protein levels.

## Role of Lys202 neddylation of PSD-95 in spine maturation

Neddylation of specific lysines can be identified by mass spectrometry, taking advantage of the mass shift of modified peptides caused by di-Gly overhangs after trypsin digestion. Unfortunately, ubiquitin and Nedd8 generate the same di-Gly remnant, precluding discrimination between ubiquitin- and Nedd8-modified peptides[28]. To overcome this limitation we generated C-terminal Nedd8 mutants (MS-Nedd8) that lead to larger overhangs after trypsination (**Supplementary Fig. 6e–g**).

We evaluated the neddylated residues of PSD-95 by mass spectrometry using immunoprecipitates obtained from HEK293 cells transfected with MS-Nedd8 and PSD-95. The lysine residues Lys202, Lys393, Lys491 and Lys624 were found neddylated. Under more stringent conditions, in the absence of proteasome inhibitors, only Lys202 was identified as neddylated. In the presence of MLN-4924, neddylation of Lys202 was not observed. When we analyzed the presence of di-Gly overhangs on endogenous PSD-95 immunopurified from neurons, we found modified Lys202 again, together with Lys211. These experiments indicate that Lys202 is the most prevalently neddylated residue in PSD-95. To further confirm this biochemical finding, we mutated the Lys202 to arginine (K202R); this resulted in decreased levels of neddylated PSD-95 under both denaturing (**Fig. 7a**) and nondenaturing conditions (**Supplementary Fig. 7a**). Lys202 is located on the second PDZ domain of PSD-95. Accordingly, a shifted neddylated band was also found when we used a construct encoding only the PDZ1-3 domains, PSD-95-(PDZ1+2+3)-6xHis. A K202R version of this construct also showed reduced neddylation (**Supplementary Fig. 7b**).

Several lines of evidence indicate that PSD-95 is present in nascent spines and plays a role in spine maturation in neuronal cultures[29]. Interestingly, whereas overexpression of PSD-95 WT promoted spine maturation, neurons transfected with PSD-95 K202R developed filopodia-like structures instead of mature spines (**Fig. 7b**), similar to neurons in which neddylation was inhibited (**Fig. 2a**). Mutation of Lys202 alone was sufficient to change the maturation-promoting function of PSD-95 to a dominant-negative property. Similar effects of PSD-95 K202R on spine development were found with molecular replacement strategies (**Supplementary Fig. 7c**) that avoid potential nonspecific effects secondary to overexpression[30]. In more mature neurons PSD-95 WT induced spine growth as described in other reports[29,31], whereas PSD-95 K202R had no effect (**Fig. 7c**).

The amino acid replacement per se could have altered the structure or function of PSD-95 independently of the neddylation deficiency. To rule out this possibility, we performed a variety of control experiments (**Supplementary Fig. 8a–e**). We found a normal postsynaptic accumulation of PSD-95 K202R (**Supplementary Fig. 8a**), and FRAP experiments showed no reduction in the recovery time after photobleaching of PSD-95 K202R versus PSD-95 WT, indicating normal trafficking to and retention in the spine (**Supplementary Fig. 8b**). In addition, classical PDZ1/2-dependent PSD-95/Kv1.4 co-clustering assays in COS7 cells[32] showed no differences between WT and mutant PSD-95 K202R in their capability to coaggregate with the potassium channel Kv1.4 (**Supplementary Fig. 8c**). Finally, co-immunoprecipitation and FRET imaging experiments indicated that the well-known PSD-95–stargazin interaction[33,34] was preserved in PSD-95 K202R (**Supplementary Fig. 8d,e**).

### Neddylation of PSD-95 Lys202 and AMPA-R neurotransmission

Overexpression of PSD-95 WT in organotypic slice cultures leads to a strong increase of AMPA-R-mediated mEPSC frequency and amplitude[35,36]. We recorded AMPA-R mEPSCs in virally transduced hippocampal organotypic slice cultures. As expected, neurons overexpressing PSD-95 WT showed increased mEPSC frequency and amplitude (**Fig. 7d**). Similar to results reported with PSD-95 knockdown strategies[16,37], PSD-95 K202R strongly reduced mEPSC frequency (**Fig. 7d**) but did not alter mEPSC amplitude (**Fig. 7d**), indicating that K202R replacement turned PSD-95 dominant negative.

Potential changes to the ubiquitylation of PSD-95 induced by Nedd8 might act as a confounding factor, but neither MLN-4924 nor the K202R replacement influenced the ubiquitylation of PSD-95 (**Supplementary Fig. 8f**).

Taken together, these findings indicate that neddylation of Lys202 is necessary for PSD-95 function.

### Synapse instability in *Nae1*$^{CamKII\alpha\text{-}CreERT2}$ mice

Next we explored the role of neddylation in forebrain excitatory circuits of the adult brain by using mouse genetics.

Nae1 is a subunit of the E1 enzyme of neddylation. To avoid the effects of neddylation on developmental stages, we generated *Nae1*$^{floxed}$ mice and crossed them with *CamKII*$\alpha^{CreERT2}$ mice to generate the *Nae1*$^{CamKII\alpha\text{-}CreERT2}$ mouse line (**Supplementary Fig. 9a,b**). In these mice, Nae1 is inactivated upon tamoxifen administration only in forebrain projection neurons (**Supplementary Fig. 9c–e**). A Thy1-EGFP reporter allele was introduced through further crossings with the Thy1-EGFP (M) line.

Three to four weeks after tamoxifen administration, *Nae1*$^{CamKII\text{-}CreERT2}$ mice displayed a severe reduction in spine density and size in both cortical and hippocampal pyramidal neurons (**Fig. 8a**). The morphological changes were limited to spines, and the general neuron morphology remained unaffected (**Supplementary Fig. 9f**). The loss of spines can be accompanied by synaptic instability; indeed, the density of VGLUT1 puncta was severely reduced in *Nae1*$^{CamKII\alpha\text{-}CreERT2}$ mice (**Fig. 8b**). To assess the strength of synaptic transmission, we compared the size of the presynaptic fiber volley (input) with the slope of the excitatory postsynaptic potential (EPSP) (output) in CA1 stratum radiatum (**Fig. 8c**). We found that synaptic transmission was dramatically reduced in *Nae1*$^{CamKII\text{-}CreERT2}$ mice, which also showed lower mRNA expression levels of activity-induced genes in cortex and hippocampus, suggesting reduced neuronal activity in these areas (**Fig. 8d**). No changes were observed in the required stimulation strength, indicating that excitability was not impaired (**Supplementary Fig. 9g**). To the best of our knowledge this is the first description of the ablation of an entire post-translational modification specifically affecting spine morphology and maintenance.

### Specific cognitive deterioration in *Nae1*$^{CamKII\alpha\text{-}CreERT2}$ mice

Next we subjected *Nae1*$^{Control}$ and *Nae1*$^{CamKII\alpha\text{-}CreERT2}$ mice to a comprehensive battery of behavioral tests. Spatial, hippocampal-dependent working memory (water-cross maze and Y-maze tests) (**Fig. 8e,f**) and the ability to remember a familiar object after either short (30 min) or long (24 h) intertrial intervals (**Fig. 8g** and **Supplementary Fig. 9h**) were impaired in *Nae1*$^{CamKII\alpha\text{-}CreERT2}$ animals. These results were not influenced by changes in locomotion (**Supplementary Fig. 9i**). Sociability, expressed as the preference for a social contact versus a non-social contact (dummy mouse), was similar in both groups (**Fig. 8h**). When the dummy mouse was exchanged for a new, unfamiliar mouse immediately after the test (social novelty), *Nae1*$^{CamKII\alpha\text{-}CreERT2}$ animals spent more time interacting with the new mouse, similar to controls (**Supplementary Fig. 9j**). This indicates that *Nae1*$^{CamKII\alpha\text{-}CreERT2}$ mice are able to discriminate familiar from unfamiliar partners and that their social exploratory behavior is preserved. However, in another experimental group, the animals previously exposed to the sociability test were retested for social memory after a 5 h interval. Control animals showed a preference for the unfamiliar mouse, but neddylation-deficient mice did not, suggesting a specific inability to recall a familiar mouse (**Fig. 8i**).

Finally, we performed fear-conditioning studies in which animals were re-exposed to the tone 24 h after conditioning and to the context 48 h after conditioning. Deficits in both cue- and context-dependent fear memories were found in *Nae1*$^{CamKII\alpha\text{-}CreERT2}$ mice (**Fig. 8j** and **Supplementary Fig. 9k**).

Even though the synaptic consequences of neddylation deficiency were pronounced, we were surprised that the strong behavioral abnormalities of *Nae1*$^{CamKII\alpha\text{-}CreERT2}$ mice across the different learning and memory paradigms were not accompanied by changes in social novelty or sociability, behaviors that also depend on intact forebrain circuits[38]. To further explore this difference, we sought to investigate anxiety as a readout for emotional behavior, since its driving circuits are also based on forebrain structures. Anxiety levels evaluated in a dark-light box (**Supplementary Fig. 9l**), in an elevated zero-maze, in an elevated plus-maze and with novelty-induced suppression of feeding (not shown) were similar in *Nae1*$^{Control}$ and *Nae1*$^{CamKII\alpha\text{-}CreERT2}$ mice, thereby confirming the overall difference between the performance in cognitive versus emotional or social behavior. However, these results argue against the possible influence of an altered anxiety response on the observed cognitive defects.

## DISCUSSION

The present findings demonstrate that neddylation is developmentally upregulated in the brain and active in synapses. We show that Nedd8 conjugation is necessary for spine maturation and stability and is critical for the function of PSD-95 in the spine. Mice carrying a specific ablation of neddylation in forebrain excitatory neurons during adulthood exhibited synaptic instability, impaired neurotransmission and cognitive deterioration.

### Neddylation controls spinogenesis during brain development

We found that Nedd8 and Hub1 had the highest mRNA expression levels among UBLs in neurons. Although Nedd8 has been described as slightly downregulated during development[4], we observed constant mRNA and protein levels of free Nedd8. These discrepancies probably stem from the semiquantitative nature of the northern blotting technique used in the original study[4]. The profiles of neddylated proteins increase during brain and neuronal maturation. Conversely,

the amount of ubiquitylated proteins in the brain decreases during the same period[39], further pointing toward a specific developmental role of neddylation beyond its cross-talk with the ubiquitylation cascade. The increase in neddylation might be due to increased expression of E3 ligases or neuronal Nedd8 targets. Alternatively, the increase in brain activity during maturation might boost neddylation. These possibilities will be a matter of further investigation.

Filopodia have been described as developmental precursors of mature spines[12–14]. We demonstrated that downregulation of the Nedd8 pathway blocked spine maturation.

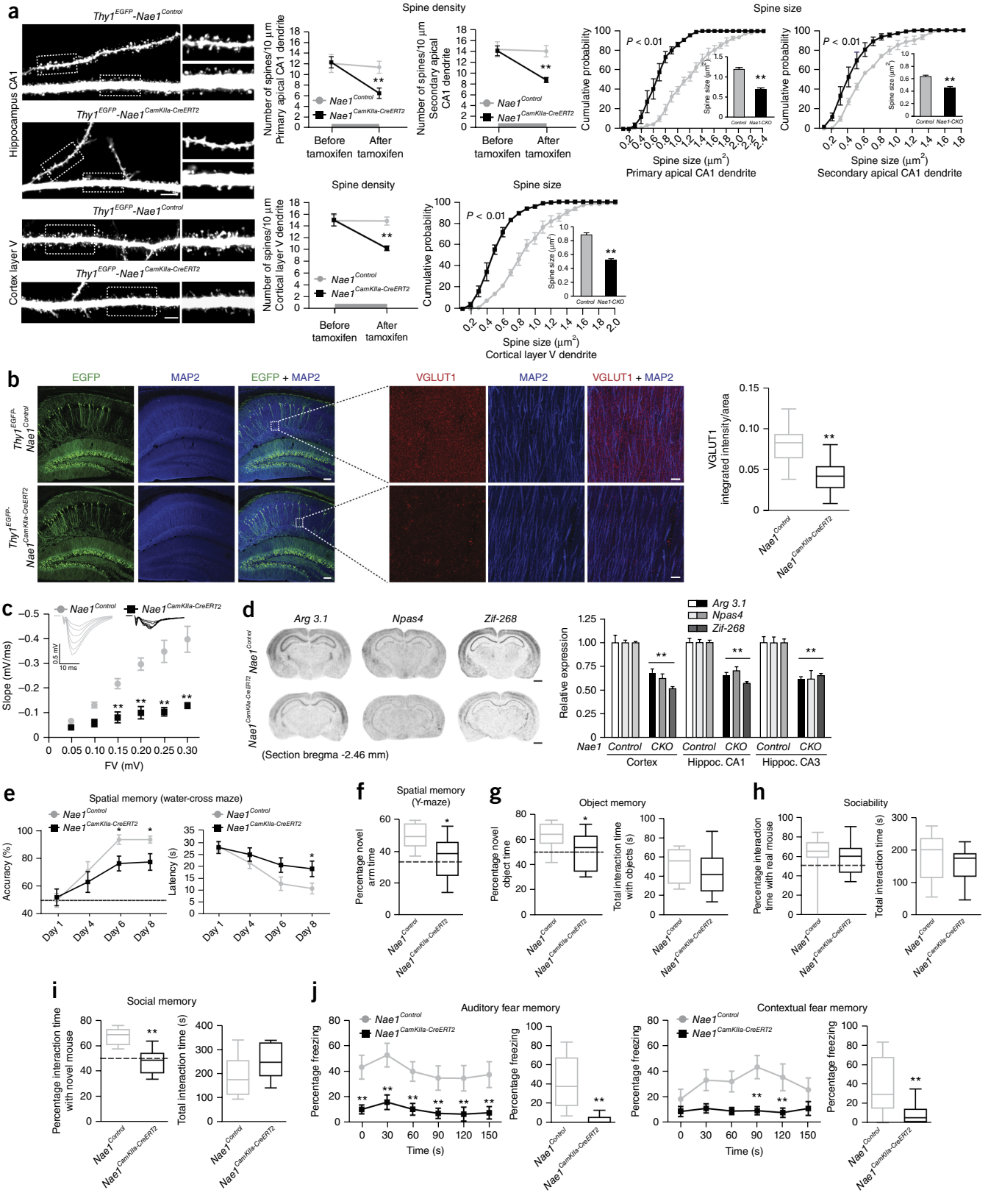

It might be argued that a nonspecific effect of neddylation inhibition (for example, on general cell metabolism) might have contributed to the observed effects. However, several findings exclude this possibility and instead indicate a rather confined effect of neddylation on postsynaptic proteins: (i) In neddylation-deficient primary neurons, synapses were still present on dendritic shafts. (ii) The amplitude of mEPSCs was not affected in Ubc12-C111S-transfected neurons, suggesting that the remaining synapses were functionally intact. (iii) MLN-4924 reduced the number of excitatory synapses but did not affect the density of adjacent GABAergic synapses. (iv) Filopodia of Ubc12-C111S-transfected neurons showed normal motility. (v) *In vivo* long-lasting ablation of the neddylation pathway in *Nae1*$^{CamKII\alpha\text{-}CreERT2}$ mice did not result in any obvious sign of neuronal damage.

### Nedd8, a new UBL within and for the synapse

We found that several substrates were specifically neddylated in the different synaptic fractions. These results represent the first description of neddylation as a post-translational modification present in the synapse. Ubc12 was enriched in the Triton-soluble fraction of the postsynaptic compartment; this positioning might be a topographical advantage for the neddylation of intraspine proteins and cross-talk with other signaling cascades.

From a mechanistic perspective, it will be critical to identify neuronal Nedd8 target proteins in order to understand the different functions of neddylation in the synapse. The discrimination of neddylated versus ubiquitylated lysine residues by mass spectrometry with trypsin digestion protocols is currently not feasible. We describe herein a new method that overcomes this problem and allowed us to identify the neddylation of Lys202 in PSD-95. The method combines simplicity and sensitivity, as it is based on a single amino-acid insertion or replacement in Nedd8; however, this strategy still requires the replacement of endogenous Nedd8 or exogenous expression of the MS-Nedd8 variant. In addition, this method might allow screenings aimed at identifying ubiquitin- and Nedd8-conjugated substrates in parallel.

Blocking neddylation for a long time led to spine elimination, but short and transient Nedd8 conjugation blockade induced spine shrinkage. The reduction in spine size was reversible in ~55% and irreversible in ~35% of analyzed spines, whereas ~10% of spines remained fully resistant to MLN-4924 treatment. These changes occurred among spines of the same neurons, indicating that neddylation exerts tight but inhomogeneous control on spine architecture and that individual spines react with individual sensitivities to changes in Nedd8 conjugation. As described for AMPARs and PSD-95 (refs. 23,37), a particular composition of proteins in individual spines (for example, Nedd8 pathway enzymes) might determine the responses of specific spine subsets to different stimuli.

Long-lasting neddylation inhibition in *Nae1*$^{CamKII\alpha\text{-}CreERT2}$ mice reduced not only spine but also synaptic density. This spine loss might have been initiated or influenced by previous destabilization of presynaptic boutons; however, a similar pattern of spine elimination was observed in *in utero* electroporated neurons. Since this approach reports essentially cell-intrinsic processes,

**Figure 8** Conditional inactivation of neddylation in principal neurons of the forebrain leads to spine loss, decreased synaptic activity and cognitive deficits. In all panels, $*P < 0.05$, $**P < 0.01$. (**a**) Reduced spine density and spine size in pyramidal neurons in the hippocampus (CA1) and cortex (layer V) after inactivation of neddylation in adult *Thy1*$^{EGFP}$-*Nae1*$^{CamKII\alpha\text{-}CreERT2}$ mice. (Spine density, two-way ANOVA, primary apical dendrite: treatment × genotype interaction, $P = 0.044$, $F_{1,96} = 4.15$; genotype, $P = 0.065$, $F_{1,96} = 3.48$; treatment, $P = 0.010$, $F_{1,96} = 6.85$. Spine density, two-way ANOVA, secondary apical dendrite: treatment × genotype interaction, $P = 0.014$, $F_{1,96} = 6.31$; genotype, $P = 0.007$, $F_{1,96} = 7.71$; treatment, $P = 0.006$, $F_{1,96} = 8.08$. Spine density, two-way ANOVA, cortical layer V: treatment × genotype interaction, $P = 0.003$, $F_{1,96} = 9.27$; genotype, $P = 0.005$, $F_{1,96} = 8.40$; treatment, $P = 0.002$, $F_{1,96} = 9.76$. Bonferroni post hoc test: primary apical dendrite, $**P = 0.0073$ for control versus *CKO* after tamoxifen; secondary apical dendrite, $**P = 0.00015$ for control versus *CKO* after tamoxifen; cortical layer V, $**P = 3.45 \times 10^{-5}$ for control versus *CKO* after tamoxifen. Spine size (distributions analyzed by Kolmogorov-Smirnov test, $**P < 0.01$; average values analyzed by two-tailed unpaired Student's *t* test): primary apical dendrite, $**P = 1.41 \times 10^{-17}$, $t_{48} = 9.64$; secondary apical dendrite, $**P = 8.4 \times 10^{-11}$, $t_{48} = 6.5$; cortical layer V, $**P = 8.22 \times 10^{-21}$, $t_{48} = 10.15$; all for control versus *CKO* after tamoxifen; $n = 25$ neurons from five animals.) Scale bars, 10 µm. (**b**) Decreased density of excitatory (VGLUT1-positive) synapses in stratum radiatum of the hippocampus (two-tailed unpaired Student's *t* test, $**P = 3.73 \times 10^{-6}$, $t_{158} = 5.51$; $n = 80$ areas from five animals). Scale bars, 100 µm (5 µm in magnified views). (**c**) Decrease in basal synaptic transmission (input-output curve) in *Nae1*$^{CamKII\alpha\text{-}CreERT2}$ mice. (Two-way ANOVA: genotype × fiber volley (FV) interaction, $P = 0.0001$, $F_{5,89} = 10.4$; genotype, $P = 0.0001$, $F_{1,89} = 167.5$; FV, $P = 0.0001$, $F_{5,89} = 33.37$. Bonferroni post hoc test: 0.15 mV, $**P = 6.14 \times 10^{-5}$; 0.20 mV, $**P = 5.67 \times 10^{-6}$; 0.25 mV, $**P = 0.0011$; 0.30 mV, $**P = 0.0024$. All for control versus *CKO*; $n = 10$ slices from four control animals, $n = 11$ slices from four *CKO* animals.) Representative sample traces are shown. (**d**) Reduced mRNA expression of the activity-induced genes *Arg3.1*, *Npas4* and *Zif-268* in cortex and hippocampus (Hippoc.) of *Nae1*$^{CamKII\alpha\text{-}CreERT2}$ mice analyzed by *in situ* hybridization. (Two-tailed unpaired Student's *t* test, *Arg*: cortex, $**P = 0.0006$, $t_{118} = 3.55$; CA1, $**P = 8.76 \times 10^{-10}$, $t_{118} = 10.18$; CA3, $**P = 3.96 \times 10^{-6}$, $t_{118} = 6.39$. Two-tailed unpaired Student's *t* test, *Npas4*: cortex, $**P = 8.49 \times 10^{-7}$, $t_{118} = 6.76$; CA1, $**P = 2.12 \times 10^{-5}$, $t_{118} = 5.44$; CA3, $**P = 0.0024$, $t_{118} = 3.56$. Two-tailed unpaired Student's *t* test, *Zif-268*: cortex, $**P = 3.3 \times 10^{-14}$, $t_{118} = 17.13$; CA1, $**P = 9.98 \times 10^{-13}$, $t_{118} = 14.48$; CA3, $**P = 8.88 \times 10^{-8}$, $t_{118} = 7.81$. All for control versus *CKO*; $n = 60$ areas from four animals.) Scale bars, 1 mm. (**e**–**j**) Deficits in learning and memory paradigms in conditional *Nae1*$^{CamKII\alpha\text{-}CreERT2}$ mice: water-cross maze (**e**) and Y-maze (**f**) (spatial memory), object recognition test (object memory, 30 min intertrial interval) (**g**), social memory test (5 h intertrial interval) (**i**) and fear memory (**j**). Sociability was not affected (**h**). (**e**) Two-way ANOVA repeated measures. Accuracy: time × genotype interaction, $P = 0.178$, $F_{3,66} = 1.69$; genotype, $P = 0.019$, $F_{1,22} = 6.44$; time, $P = 0.0001$, $F_{3,66} = 16.74$. Latency: time × genotype interaction, $P = 0.140$, $F_{3,66} = 1.89$; genotype, $P = 0.045$, $F_{1,22} = 4.53$; time, $P = 0.0001$, $F_{3,66} = 11.81$. Bonferroni post hoc test, accuracy: day 6, $*P = 0.014$; day 8, $*P = 0.033$. Bonferroni post hoc test, latency: day 8, $*P = 0.022$. All for control versus *CKO*. (**f**–**i**) Two-tailed unpaired Student's *t* test, Y-maze (**f**), $*P = 0.014$, $t(22) = 2.69$. Two-tailed unpaired Student's *t* test, object memory (**g**): percentage novel object time, $*P = 0.045$, $t_{22} = 2.11$; total interaction time, $P = 0.439$, $t_{22} = 0.79$. Two-tailed unpaired Student's *t* test, sociability (**h**): percentage interaction time with real mouse, $P = 0.811$, $t_{22} = 0.24$; total interaction time, $P = 0.297$, $t_{22} = 1.07$. Two-tailed unpaired Student's *t* test, social memory (**i**): percentage interaction time with novel mouse, $**P = 0.0003$, $t_{22} = 4.69$; total interaction time, $P = 0.116$, $t_{22} = 1.64$. (**j**) Two-way ANOVA repeated measures, auditory fear memory: genotype × time interaction, $P = 0.810$, $F_{5,110} = 0.45$; genotype, $P = 0.002$, $F_{1,22} = 12.12$; time, $P = 0.0024$, $F_{5,110} = 3.91$. Two-way ANOVA repeated measures, contextual fear memory: genotype × time interaction, $P = 0.013$, $F_{5,110} = 3.04$; genotype, $P = 0.007$, $F_{1,22} = 8.42$; time, $P = 0.0169$, $F_{5,110} = 2.88$. Bonferroni post hoc test, auditory fear memory: 0 s, $**P = 0.0017$; 30 s, $**P = 0.0017$; 60 s, $**P = 0.005$; 90 s, $**P = 0.009$; 120 s, $**P = 0.008$; 150 s, $**P = 0.005$. Bonferroni post hoc test, contextual fear memory: 90 s, $**P = 0.00055$; 120 s, $*P = 0.003$. All for control versus *CKO*. Two-tailed unpaired Student's *t* test: auditory fear memory, $**P = 6.9 \times 10^{-6}$, $t_{22} = 5.23$; contextual fear memory, $**P = 0.0035$, $t_{22} = 3.27$. Control versus *CKO*; $n = 12$ animals per group. For all experiments (**a**–**j**) *Nae1*$^{Control}$ and *Nae1*$^{CamKII\alpha\text{-}CreERT2}$ mice received tamoxifen in food during postnatal week 7 and 8, and analyses were performed 3–4 weeks later. Data are presented as mean ± s.e.m. and box-and-whisker plots (box limits represent first and third quartiles, center line represents median, and whiskers represent minimum and maximum values).

it seems that the sole inhibition of neddylation in the postsynaptic neuron is sufficient to induce spine elimination.

As a consequence of the loss of spines, synapses may be either eliminated or transformed into dendritic shaft synapses. Although it cannot be entirely ruled out, this last scenario seems unlikely given the results of long-lasting *in vivo* two-photon experiments comparing the numbers of disappearing spines and existing shaft synapses[40].

### PSD-95 neddylation as a molecular proof of principle

As mentioned, it is probably unrealistic to assume that neddylation of a single protein could explain the effects triggered by the entire Nedd8 pathway. Yet the fact that the neddylation-deficient variant PSD-95 Lys202 recapitulated the effects of Nedd8 inhibition on spine maturation suggests that neddylation of PSD-95 is important for at least some of the observed effects.

From a mechanistic point of view, we showed that neddylation of PSD-95 requires the N-terminal PEST domain of the scaffolding protein, a motif that is also needed for the association of PSD-95 and Ubc12. Furthermore, PSD-95 neddylation not only decreased with MLN-4924 treatment but also increased in Nedp-1 knockout neurons, suggesting that this deneddylase removes Nedd8 from conjugated PSD-95. Our results indicate that PSD-95 neddylation, which is mediated by Mdm2 in a PEST motif–dependent manner, controls the function of PSD-95 on synapse maturation and AMPA neurotransmission but does not affect its degradation rates. Notably, Mdm2 also triggers the ubiquitylation of PSD-95 with PEST-motif dependence, leading to PSD-95 degradation and NMDA-induced AMPAR endocytosis[21,22,41]. However, neddylation does not influence PSD-95 ubiquitylation. Together these findings suggest that Mdm2 might control the stability or specific functions of PSD-95 by controlling the Nedd8 and/or ubiquitin load of the scaffolding protein.

Whereas MLN-4924 reduced the PSD-95 content in the synaptic density, similar effects were not recapitulated by PSD-95 K202R, suggesting that neddylation of other PSD-95-associated proteins is needed for the clustering of PSD-95. This is not surprising because the homo-oligomerization of PSD-95 is not sufficient for its clustering, and therefore other associated proteins are necessary for its aggregation in puncta-like structures[32,42].

In neuronal cultures, the number and size of spines increases with PSD-95 overexpression[29] and decreases after PSD-95 knockdown[16]. Surprisingly, the K202R mutation rendered PSD-95 dominant negative, which reduced spine density and increased the number of filopodia. Lys202 resides in the second PDZ domain, and mutations of this domain also confer dominant-negative properties to PSD-95 and induce the formation of elongated protrusions[43].

From a functional perspective, acute PSD-95 knockdown in hippocampal slice cultures decreases frequency with no change in amplitude of mEPSCs, suggesting that only a subpopulation of synapses is silenced[16,37]. PSD-95 K202R–transduced neurons showed no reduction in the amplitude of mEPSCs but showed a large decrease in the event frequency. These results mimicked the effects observed with PSD-95 knockdown, suggesting that neddylation of PSD-95 Lys202 is necessary for the proactive function of PSD-95 in the transition from silent to mature AMPAR-containing spines.

The PSD-95 K202R mutant showed either lack of function (spine size) or dominant-negative properties (spine development and AMPAR-mediated mEPSCs). Thus, neddylated Lys202 would be permissive for some functions of PSD-95 or crucial for others, likely owing to differential interaction with PSD-95 partners involved in those processes.

The intrinsic molecular promiscuity of PSD-95 prevents an obvious selection of one or two candidate binding proteins to explain the effects observed with PSD-95 K202R. We speculated on a potential interference with stargazin, a well-known PSD-95 interactor that stabilizes postsynaptic AMPARs, but K202R replacement did not alter this interaction . Yet other PSD-95 partners, such as TARPs γ3, γ4 and γ8; the adhesion molecule Salm 2; the actin organizer Kalirin-7; and the signaling proteins SynGAP, RalBP1 and DGKζ, which also bind to PDZ1-2 and regulate synaptic differentiation or AMPAR dynamics, might be involved in the effects of neddylated PSD-95 (refs. 24,43–46). Further proteomic and molecular studies will be necessary in order for this question to be answered.

### From structure to function in *Nae1*$^{CamKII\alpha\text{-}CreERT2}$ mice

The generation of *Nae1*$^{CamKII\alpha\text{-}CreERT2}$ mice allowed us to restrict the *Nae1* deletion to mature excitatory forebrain neurons. After tamoxifen-induced *Nae1* gene deletion, morphological alterations were found only at the spine level, similarly to phenotypes observed in other knockout models of spine-enriched proteins[47–49]. To the best of our knowledge, this is the first description of the ablation of an entire post-translational pathway specifically affecting spine morphology and maintenance. Spine elimination was not accompanied by any sign of cell damage; this is remarkable, as 4 weeks of *in vivo* peripheral MLN-4924 administration triggers apoptosis in highly replicating cells[7]. These differences show that neddylation adopts more sophisticated molecular functions as differentiation progresses. This pathway has been mainly investigated as a regulator of cullin-RING complexes in the context of cell cycle and proliferation, but the data presented here suggest that many functions and targets of neddylation in fully differentiated postmitotic cells are still unknown.

Similar to other knockout mouse models for structurally relevant postsynaptic proteins (for example, Arp2, Arp3, Kalirins and Shank1)[47–49], *Nae1*$^{CamKII\alpha\text{-}CreERT2}$ mice developed severe spine defects accompanied only by impairments in specific behavioral tests, and not by a generalized alteration of behavior. However, this behavioral profile presented a notable feature: although severe learning and memory deficits were observed in *Nae1*$^{CamKII\alpha\text{-}CreERT2}$ mice, results were not altered in other tests assessing social novelty, sociability or anxiety-related behavior. This is puzzling, since the analyzed emotional and social responses also depend on the limbic structures targeted in *Nae1*$^{CamKII\alpha\text{-}CreERT2}$ animals. From a perspective focused on the structural alteration of the synapse, these learning- and memory-specific deficits may imply that cognitive tasks demand the use of neurons with intact synaptic capabilities, whereas social and emotional behaviors can be adequately driven by circuits with a lower degree of synaptic strength or connectivity. Nevertheless, at faster temporal scales, neddylation plausibly exerts additional functional effects on neurotransmission, which would also affect circuit function and possibly behavior. Therefore, a more comprehensive understanding of the role of neddylation in neuronal activity will be necessary before this question can be addressed.

Nedd8 has been found in inclusion bodies involved in degenerative diseases[50], and neddylation increases the activity of Parkin and stabilizes Pink, two proteins associated with Parkinson disease[8]. The fact that deficits in neddylation trigger synaptic instability and cognitive dysfunction makes neddylation an attractive candidate for further exploration in the context of neurodegenerative disorders.

In conclusion, the findings presented here show that neddylation is active in dendritic spines, reveal that many unidentified synaptic proteins are neddylated and define PSD-95 neddylation as a proof of principle of the functional relevance of neddylation on synaptic

proteins. Moreover, they suggest that neddylation is a key regulator of synapse maturation and spine stability and thus influences neurotransmission and cognitive behavior. In summary, these results demonstrate that neddylation represents a relevant, as yet unexplored post-translational regulatory pathway controlling the structure and function of synapses.

## METHODS

Methods and any associated references are available in the online version of the paper.

*Note: Any Supplementary Information and Source Data files are available in the online version of the paper.*


### ACKNOWLEDGMENTS

We thank S. Bauer, A. Moebus, C. Mattusch, K. Henes, D. Glass and S. Opitz for their technical assistance; the Bordeaux Imaging Center and C. Poujol for assistance with FRET experiments; and R. Malenka, P. Scheiffele, C. Sala, V.R. Wedlich-Soeldner, V. Tarabykin, D.C. Lie, W. Snider, T. Soderling, Y. Yarden and J.W. Conaway for providing plasmids. We are grateful to P. Scheiffele and R. Klein for helpful comments and advice. This work was supported by ERC grant Nano-Dyn-Syn (D.C. and A.-S.H.); the Helmholtz Alliance for Mental Health (D.M.V.-W.); BMBF grant nos. NGNFplus 01GS08174-14 (D.M.V.-W.), 01GS08151 and 01GS08155 (J.M.D.); the DFG SPP1365 grant (D.R.); and the Max Planck Society (J.M.D. and D.R.).


### AUTHOR CONTRIBUTIONS

A.M.V. and M.M.B. designed and performed the experiments and interpreted the results. S.A.G., C.A.V., J.S.R., C.A.B., N.D. and F.R. performed experiments. G.M. and C.W.T. performed mass spectrometry experiments. A.-S.H. and D.C. performed FRET and FRAP studies. V.S. designed electrophysiology experiments and helped write the manuscript. D.M.V.-W., C.T.W. and J.M.D. analyzed the data. D.R. supervised the project and developed the conceptual and experimental framework. A.M.V. and D.R. wrote the manuscript.

### COMPETING FINANCIAL INTERESTS

The authors declare no competing financial interests.




1. Kawabe, H. & Brose, N. The role of ubiquitylation in nerve cell development. *Nat. Rev. Neurosci.* **12**, 251–268 (2011).
2. Yang, Y., Kim, A.H. & Bonni, A. The dynamic ubiquitin ligase duo: Cdh1-APC and Cdc20-APC regulate neuronal morphogenesis and connectivity. *Curr. Opin. Neurobiol.* **20**, 92–99 (2010).
3. van der Veen, A.G. & Ploegh, H.L. Ubiquitin-like proteins. *Annu. Rev. Biochem.* **81**, 323–357 (2012).
4. Kumar, S., Tomooka, Y. & Noda, M. Identification of a set of genes with developmentally down-regulated expression in the mouse-brain. *Biochem. Biophys. Res. Commun.* **185**, 1155–1161 (1992).
5. Xirodimas, D.P. Novel substrates and functions for the ubiquitin-like molecule NEDD8. *Biochem. Soc. Trans.* **36**, 802–806 (2008).
6. Petroski, M.D. & Deshaies, R.J. Function and regulation of cullin-RING ubiquitin ligases. *Nat. Rev. Mol. Cell Biol.* **6**, 9–20 (2005).
7. Soucy, T.A. *et al.* An inhibitor of NEDD8-activating enzyme as a new approach to treat cancer. *Nature* **458**, 732–736 (2009).
8. Choo, Y.S. *et al.* Regulation of parkin and PINK1 by neddylation. *Hum. Mol. Genet.* **21**, 2514–2523 (2012).
9. Djagaeva, I. & Doronkin, S. Dual regulation of dendritic morphogenesis in *Drosophila* by the COP9 signalosome. *PLoS ONE* **4**, e7577 (2009).
10. Stadler, C. *et al.* Immunofluorescence and fluorescent-protein tagging show high correlation for protein localization in mammalian cells. *Nat. Methods* **10**, 315–323 (2013).
11. Wada, H., Yeh, E.T. & Kamitani, T. A dominant-negative UBC12 mutant sequesters NEDD8 and inhibits NEDD8 conjugation in vivo. *J. Biol. Chem.* **275**, 17008–17015 (2000).
12. Ziv, N.E. & Smith, S.J. Evidence for a role of dendritic filopodia in synaptogenesis and spine formation. *Neuron* **17**, 91–102 (1996).
13. Fiala, J.C., Feinberg, M., Popov, V. & Harris, K.M. Synaptogenesis via dendritic filopodia in developing hippocampal area CA1. *J. Neurosci.* **18**, 8900–8911 (1998).
14. Yuste, R. & Bonhoeffer, T. Genesis of dendritic spines: insights from ultrastructural and imaging studies. *Nat. Rev. Neurosci.* **5**, 24–34 (2004).
15. Lohmann, C., Finski, A. & Bonhoeffer, T. Local calcium transients regulate the spontaneous motility of dendritic filopodia. *Nat. Neurosci.* **8**, 305–312 (2005).
16. Ehrlich, I., Klein, M., Rumpel, S. & Malinow, R. PSD-95 is required for activity-driven synapse stabilization. *Proc. Natl. Acad. Sci. USA* **104**, 4176–4181 (2007).
17. Yoshihara, Y., De, R.M. & Muller, D. Dendritic spine formation and stabilization. *Curr. Opin. Neurobiol.* **19**, 146–153 (2009).
18. Verpelli, C., Schmeisser, M.J., Sala, C. & Boeckers, T.M. Scaffold proteins at the postsynaptic density. *Adv. Exp. Med. Biol.* **970**, 29–61 (2012).
19. Bayés, A. & Grant, S.G. Neuroproteomics: understanding the molecular organization and complexity of the brain. *Nat. Rev. Neurosci.* **10**, 635–646 (2009).
20. Chan, Y. *et al.* DEN1 deneddylates non-cullin proteins in vivo. *J. Cell Sci.* **121**, 3218–3223 (2008).
21. Colledge, M. *et al.* Ubiquitination regulates PSD-95 degradation and AMPA receptor surface expression. *Neuron* **40**, 595–607 (2003).
22. Tsai, N.P. *et al.* Multiple autism-linked genes mediate synapse elimination via proteasomal degradation of a synaptic scaffold PSD-95. *Cell* **151**, 1581–1594 (2012).
23. Opazo, P., Sainlos, M. & Choquet, D. Regulation of AMPA receptor surface diffusion by PSD-95 slots. *Curr. Opin. Neurobiol.* **22**, 453–460 (2012).
24. Han, K. & Kim, E. Synaptic adhesion molecules and PSD-95. *Prog. Neurobiol.* **84**, 263–283 (2008).
25. Shepherd, J.D. & Huganir, R.L. The cell biology of synaptic plasticity: AMPA receptor trafficking. *Annu. Rev. Cell Dev. Biol.* **23**, 613–643 (2007).
26. Bingol, B. & Schuman, E.M. A proteasome-sensitive connection between PSD-95 and GluR1 endocytosis. *Neuropharmacology* **47**, 755–763 (2004).
27. Ehlers, M.D. Activity level controls postsynaptic composition and signaling via the ubiquitin-proteasome system. *Nat. Neurosci.* **6**, 231–242 (2003).
28. Kirkpatrick, D.S., Denison, C. & Gygi, S.P. Weighing in on ubiquitin: the expanding role of mass-spectrometry-based proteomics. *Nat. Cell Biol.* **7**, 750–757 (2005).
29. El-Husseini, A.E., Schnell, E., Chetkovich, D.M., Nicoll, R.A. & Bredt, D.S. PSD-95 involvement in maturation of excitatory synapses. *Science* **290**, 1364–1368 (2000).
30. Schlüter, O.M., Xu, W.F. & Malenka, R.C. Alternative N-terminal domains of PSD-95 and SAP97 govern activity-dependent regulation of synaptic AMPA receptor function. *Neuron* **51**, 99–111 (2006).
31. Sturgill, J.F., Steiner, P., Czervionke, B.L. & Sabatini, B.L. Distinct domains within PSD-95 mediate synaptic incorporation, stabilization, and activity-dependent trafficking. *J. Neurosci.* **29**, 12845–12854 (2009).
32. Hsueh, Y.P., Kim, E. & Sheng, M. Disulfide-linked head-to-head multimerization in the mechanism of ion channel clustering by PSD-95. *Neuron* **18**, 803–814 (1997).
33. Schnell, E. *et al.* Direct interactions between PSD-95 and stargazin control synaptic AMPA receptor number. *Proc. Natl. Acad. Sci. USA* **99**, 13902–13907 (2002).
34. Sainlos, M. *et al.* Biomimetic divalent ligands for the acute disruption of synaptic AMPAR stabilization. *Nat. Chem. Biol.* **7**, 81–91 (2011).
35. Ehrlich, I. & Malinow, R. Postsynaptic density 95 controls AMPA receptor incorporation during long-term potentiation and experience-driven synaptic plasticity. *J. Neurosci.* **24**, 916–927 (2004).
36. Stein, V., House, D.R.C., Bredt, D.S. & Nicoll, R.A. Postsynaptic density-95 mimics and occludes hippocampal long-term potentiation and enhances long-term depression. *J. Neurosci.* **23**, 5503–5506 (2003).
37. Elias, G.M. *et al.* Synapse-specific and developmentally regulated targeting of AMPA receptors by a family of MAGUK scaffolding proteins. *Neuron* **52**, 307–320 (2006).
38. Felix-Ortiz, A.C. & Tye, K.M. Amygdala inputs to the ventral hippocampus bidirectionally modulate social behavior. *J. Neurosci.* **34**, 586–595 (2014).
39. Chen, P.C. *et al.* Ubiquitin homeostasis is critical for synaptic development and function. *J. Neurosci.* **31**, 17505–17513 (2011).
40. Trachtenberg, J.T. *et al.* Long-term in vivo imaging of experience-dependent synaptic plasticity in adult cortex. *Nature* **420**, 788–794 (2002).
41. Bianchetta, M.J., Lam, T.T., Jones, S.N. & Morabito, M.A. Cyclin-dependent kinase 5 regulates PSD-95 ubiquitination in neurons. *J. Neurosci.* **31**, 12029–12035 (2011).
42. Christopherson, K.S. *et al.* Lipid- and protein-mediated multimerization of PSD-95: implications for receptor clustering and assembly of synaptic protein networks. *J. Cell Sci.* **116**, 3213–3219 (2003).
43. Nonaka, M., Doi, T., Fujiyoshi, Y., Takemoto-Kimura, S. & Bito, H. Essential contribution of the ligand-binding beta B/beta C loop of PDZ1 and PDZ2 in the regulation of postsynaptic clustering, scaffolding, and localization of postsynaptic density-95. *J. Neurosci.* **26**, 763–774 (2006).
44. Han, K. *et al.* Regulated RalBP1 binding to RalA and PSD-95 controls AMPA receptor endocytosis and LTD. *PLoS Biol.* **7**, e1000187 (2009).
45. Kim, K. *et al.* Synaptic removal of diacylglycerol by DGKzeta and PSD-95 regulates dendritic spine maintenance. *EMBO J.* **28**, 1170–1179 (2009).
46. Xie, Z. *et al.* Kalirin-7 controls activity-dependent structural and functional plasticity of dendritic spines. *Neuron* **56**, 640–656 (2007).
47. Kim, I.H. *et al.* Disruption of Arp2/3 results in asymmetric structural plasticity of dendritic spines and progressive synaptic and behavioral abnormalities. *J. Neurosci.* **33**, 6081–6092 (2013).
48. Hung, A.Y. *et al.* Smaller dendritic spines, weaker synaptic transmission, but enhanced spatial learning in mice lacking Shank1. *J. Neurosci.* **28**, 1697–1708 (2008).
49. Cahill, M.E. *et al.* Kalirin regulates cortical spine morphogenesis and disease-related behavioral phenotypes. *Proc. Natl. Acad. Sci. USA* **106**, 13058–13063 (2009).
50. Dil Kuazi, A. *et al.* NEDD8 protein is involved in ubiquitinated inclusion bodies. *J. Pathol.* **199**, 259–266 (2003).

## ONLINE METHODS

**Plasmids and antibodies.** pcDNA3-FLAG-human Ubc12-WT and FLAG-human Ubc12-C111S were kind gifts from J. Yarden. The dominant-negative Ubc12-C111S forms a stable heterodimeric complex with Nedd8 that is then sequestered and cannot be conjugated to target proteins[11]. Dominant-negative cullins, which lack the C-terminal region containing the conserved lysine residue[51], were obtained from Addgene. cDNAs encoding Rbx1-WT and -C42S/C45S[52], kindly given by J. W. Conaway, were subcloned into a pcDNA-3xFLAG vector. Myr-Venus was a kind gift from V. Tarabykin. The mRFP-β-actin plasmid was kindly provided by T. Soderling. The Kv1.4-HA and HA-Shank1A, -1B, -2 and -3 plasmids were kind gifts from C. Sala. Lifeact-GFP was kindly given by R. Wedlich-Soldner. Ubc12 and Nedd8 full-length ORFs were cloned from mouse brain cDNA and introduced into pcRII-TOPO and pcDNA3.1 vectors (Invitrogen). 3xFLAG-, HA- and 6xHis-BIO-tagged mouse Nedd8 were constructed in pcDNA3.1. 3xFLAG-tagged MS-Nedd8 constructs were generated from WT Nedd8 (-RGG) by insertion of an Ala (-AGG) or a Val (-VGG) at position 74, or by exchanging Leu at position 73 with Arg at position 74 (-LGG) through site-directed mutagenesis. Venus- and HA-tagged human Ubc12 and Venus-tagged mouse Nedd8 sequences were cloned in pcDNA3.1. The FLAG-Ubc12-C111S cDNA was cloned into CAG-IRES-mRFP and CAG-IRES-GFP plasmids, which were kindly provided by C. Lie. shRNA vectors targeting mouse Nedd8, Ubc12, and Rbx1, as well as a -shRNA control, were purchased from Sigma-Aldrich. Nedd8 (NM_008683): shRNA 1, ATT-GAG-ATA-GAC-ATC-GAA; shRNA 2, CTG-CCA-ATC-ATA-ATG-TGG-CAT-GAG; shRNA 3, GCG-GCT-CAT-CTA-CAG-TGG-CAA; shRNA 4, CAA-GCA-AAT-GAA-TGA-TGA-GAA; shRNA 5, CCA-CAG-ACA-AGG-TGG-AGC-GAA. Ubc12 (NM_145578): shRNA 1, CCT-TAC-GAT-AAA-CTC-CAT-AAT; shRNA 2, CCT-CAA-CTT-CAA-GCT-GGT-GAT; shRNA 3, GCA-AGT-TTG-TAT-TCA-GCT-TTA; shRNA 4, GCG-CTC-CAT-GAG-AGG-TGG-TTA; shRNA 5, CCA-AGG-TGA-AGT-GTG-AAA-CAA. Rbx1 (NM_019712): shRNA 1, CCG-TGT-TCA-ATT-GCT-GGC-ATA; shRNA 2, CCT-GGG-ACA-TTG-TGG-TTG-ATA; shRNA 3, CCA-CAT-TAT-GGA-TCT-TTG-TAT; shRNA 4, GAG-TGG-GAG-TTC-CAG-AAG-TAT; shRNA 5, CCG-AAG-AGT-GTA-CGG-TTG-CAT. To generate shRNA-resistant forms of Nedd8 and Ubc12, we introduced silent mutations in the WT sequences of Nedd8 and Ubc12 in pcDNA3.1: Nedd8, tAAaCAgATGAAcGAcGAaAA; Ubc12, gCTgAAtTTtAAaCTcGTcAT. Inducible LacZ and inducible Ubc12-C111S-IRES-LacZ constructs (CAG-floxed STOP-IRES-β-galactosidase and CAG-floxed STOP-FLAG-Ubc12-C111S-IRES-β-galactosidase, respectively) were constructed. An inducible FLAG-human Ubc12-C111S-IRES-GFP construct was generated based on the pCALNL-GFP vector (Addgene). Mouse PSD-95 WT, mouse PSD-95 WT-BIO-6xHis and mouse PSD-95 (PDZ1+2+3) WT-6xHis constructs were cloned into pcDNA3.1 (Invitrogen). Mouse PSD-95 WT, mouse PSD-95 WT-BIO-6xHis, rat PSD-95 WT-EGFP and PSD-95 (PDZ1+2+3) WT plasmids were used to generate Lys202 to Arg mutation (K202R). To generate the -PEST-PSD-95 plasmid, we deleted the 12 amino acids composing the PEST motif (RYQDEDTPPLEH)[21] of rat PSD-95-WT-EGFP. To generate a mutated PEST-domain PSD-95 construct, we introduced the following mutations (underlined sequence): (MDCLCIVTTRRAEQKLISEEDLGRA). The pSUPER shRNA PSD-95 plasmid (GGA-CAT-CCA-GGC-ACA-CAA-G) was a kind gift from R. Malenka. The pSUPER shRNA control plasmid expresses a scrambled version of the shRNA sequence. For molecular replacement experiments with PSD-95, we introduced point mutations (GGAtATtCAaGCgCAtAAG) in PSD-95 WT-EGFP and PSD-95 K202R-EGFP plasmids as previously described[30]. PSD-93-GFP, SAP-97-GFP, SAP102-GFP, Homer-GFP and GKAP-GFP were cloned into pEGFP vectors (Clontech). HA-ubiquitin, myc-Mdm2-WT and Mdm-C464A constructs were obtained from Addgene. The FRET pair used was previously described[34]. Antibodies used in this study are available in **Supplementary Table 1**.

**Animals.** Mice were group-housed under standard laboratory conditions (22 ± 1 °C, 55% ± 5% humidity) with a 12:12 h light:dark schedule with food and water *ad libitum*. Mice for behavioral experiments were single-housed 2 weeks before and during the experiments under standard laboratory conditions. For staging of embryos, the day of the vaginal plug was designated embryonic day 0.5 (E0.5). The day of birth was designated postnatal day 0 (P0). For *in utero* electroporation experiments, tamoxifen (Sigma-Aldrich) was applied as previously described[53]. For all experiments with conditional Nae1 knockout mice, tamoxifen was given in food pellets (LAS CRdiet CreActive TAM400, LASvendi) during postnatal week 7/8, and the analyses were performed 3–4 weeks later. When collecting tissues and dissociated cells, we handled animals according to the Guide for the Care and Use of Laboratory Animals of the Government of Bavaria, Germany. Animal experiments were done in accordance with local regulations and the NRC Guide for the Care and Use of Laboratory Animals followed at IBioBA-CONICET and approved by the local Institutional Animal Care and Use Committee.

**Generation of the *Ubc12-LacZ* reporter, *Nae1*$^{CamKII\alpha\text{-}CreERT2}$ and *Nedp1*-knockout mouse lines.** The Ubc12- and Nedp1-GGTC-ES cell clones were generated by the International Knockout Mouse Consortium (IKMC) (https://www.mousephenotype.org/). The integration sites were confirmed by Splinkerette-PCR. For the conditional knockout of the *Nae1* gene (ENSMUSG00000031878), a targeted embryonic stem (ES) cell clone (EPD0441_1_B07; JM8A3.N1) was obtained from Eucomm. Mutant ES cells were used to generate chimeric mice by BALB/c blastocyst injection. Germline transmission of the modified alleles was confirmed in offspring from male chimeras bred to WT C57BL/6J mice. In the case of the Nae1 mice, the offspring of the chimeras were bred first to hACTB::FLP mice[54], then to CamKIIα-CreERT2 (ref. 55) and Thy1-EGFP (M)[56] mice. Primers for genotyping by PCR are available in **Supplementary Table 2**.

***In situ* hybridization.** ISH was performed on C57BL/6, *Nae1*$^{Control}$ and *Nae1*$^{CamKII\alpha\text{-}CreERT2}$ mouse brain sections as previously described[53]. The following riboprobes were used: Ubc12, nucleotides 248–799 of GenBank accession number NM_145578.3; Nedd8, nucleotides 95–340 of GenBank accession number NM_008683; Arg3.1, nucleotides 671–1532 of GenBank accession number NM_018790.1; Npas4, nucleotides 1480–2323 of GenBank accession number NM_153553.4; and Zif-268, nucleotides 245–786 of GenBank accession number NM_007913.

**LacZ staining, DAB immunohistochemistry and immunofluorescence staining.** X-Gal and immunofluorescence stainings were performed as previously described[53,57], with some modifications.

**RNA isolation and qRT-PCR.** cDNA was generated from total RNA, isolated with TRIzol, with Reverse Trancriptase Superscript II and oligo-dT primers (Invitrogen). qRT-PCR was performed with a Light Cycler (Roche) and the QuantiFast SYBR Green PCR Kit (Qiagen). Rpl19 and Gapdh were used as housekeepers. The primers used are listed in **Supplementary Table 2**.

**Primary cell cultures and transfection of primary neurons.** Primary hippocampal and cortical neurons were prepared from CD1 mouse or Sprague-Dawley rat embryos (E17.5–E19.5) and maintained in Neurobasal-A medium with 2% B27 and 0.5 mM GlutaMAX-I (Gibco) at 37 °C and 5% $CO_2$ (ref. 58). Neurons were transfected via calcium phosphate. When necessary, neurons were cultured on primary cerebral astrocytes, isolated from P1 CD1 mouse pups[59]. MLN-4924 (Active Biochem) was used at 1 μM unless otherwise stated. 4-OH-tamoxifen (Sigma-Aldrich) was used at a final concentration of 0.5 μM. For immunoprecipitation experiments with BIO-Nedd8, neurons were nucleofected (Amaxa), and the medium was supplemented with 4 μM Biotin (Sigma-Aldrich). For experiments involving fluorescence resonance energy transfer (FRET) and fluorescence recovery after photobleaching microscopy (FRAP), transfections were performed at DIV9–11 with Effectene (Qiagen).

**Culture of cell lines and transient transfections.** HEK293, Neuro-2a and COS-7 cells were grown in Dulbecco's modified Eagle's medium (DMEM) supplemented with 10% fetal calf serum, penicillin (100 units/ml), streptomycin (100 μg/ml) and 2 mM L-glutamine (Gibco) at 37 °C and 5% $CO_2$. Cells were transiently transfected using Lipofectamine 2000 (Invitrogen). 24 to 36 h after transfection, cells were treated with vehicle, 1 μM MLN-4924 and/or 20 μM MG-132 (Merck). For experiments with BIO-tagged constructs, 4 μM biotin was added to the medium.

**Image acquisition and analysis of neuronal morphology.** Images were captured with an Olympus IX81 inverted laser scanning confocal microscope and Fluoview 1000 software. Experiments were analyzed with ImageJ (http://rsbweb.nih.gov/ij/). For spine analysis, between 250 and 800 protrusions were scored per




doi:10.1038/nn.3912

experimental group and expressed per 10 to 50 µm segment of dendrites. Dendritic protrusions were classified as either filopodia (long and thin protrusions ≥ 0.5 µm, without bulbous heads) or dendritic spines (≥0.5 µm protrusions with distinct bulbous heads)[60]. The length and width of dendritic spines were measured as described previously[61,62]. Dendritic protrusions that could not be adequately seen or whose total length exceeded 10 µm were excluded from analysis. We analyzed postsynaptic puncta by counting the number of puncta per 10 or 20 µm segment of dendrites. Mean PSD-95 immunofluorescence signal intensities were measured in single slices of the Z-stacks, in which puncta appeared brightest, with background intensity values subtracted. For the PSD-95xKv1.4 cluster assay in COS-7 cells, the sum of the areas of all clusters within a cell was divided by the total area of the cell. For quantification of the excitatory synaptic marker VGLUT1 in brain sections, images were manually thresholded to define puncta, and the total integrated intensity of puncta per tissue area was measured. For quantification of ISH signals, X-ray films were digitized, and relative levels of mRNA were determined via computer-assisted optical densitometry (ImageJ).

**Time-lapse analysis of filopodia dynamics and spine stability.** Live-cell imaging was performed with an environment-control chamber (Pecon) that maintained the neurons, cultured on glass-bottom dishes (35 mm MatTEK), at 37 °C and 5% $CO_2$. For analysis of filopodia dynamics, we recorded time-lapse movies and measured the length of individual filopodia in consecutive images over the entire time-lapse session. The motility score was defined as the average of absolute values of changes in filopodia length, as described previously[12]. For spine stability analysis, spines on dendritic segments were repeatedly imaged before, during and after MLN-4924 treatment for up to 8 h. Individual spines were manually traced in each confocal Z-stack, and the spine size ($\mu m^2$) was measured. For the spine stability experiment shown in **Figure 4c**,**d**, spines from three independent experiments were analyzed and grouped into types I, II and III according to the following criteria: type I, spines that shrank at least 15% in size during MLN-4924 treatment and recovered by at least 15% in size 70 and 120 min after MLN-4924 washout; type II, spines that shrank at least 15% in size during MLN-4924 treatment and continued to shrink or did not change during washout; and type III, spines that did not significantly change in size during the whole experiment.

***In utero* electroporation.** IUE of CD1 mouse embryos was performed as previously described[63], with minor modifications. In the case of *CamKIIα*$^{CreERT2}$ breedings[55] (CD1×C57BL/6), the litters were genotyped by PCR. Primer sequences are available in **Supplementary Table 2**.

**Organotypic hippocampal slice culture and Semliki Forest virus (SFV) infection.** PSD-95-WT-EGFP, PSD-95-K202R-EGFP and Control-EGFP were cloned into the pSFV plasmid. SFV was produced in Syrian hamster kidney cells (BHK21). Mouse hippocampal slice cultures were prepared from P7 mice as previously described[64]. Slices for mEPSC recordings were infected with SFV at DIV7–8. Virus solution was injected near CA1 using a Nanoject. mEPSC recordings were obtained 1–2 days after viral infection.

**Slice preparation for electrophysiological recordings.** Animals were anesthetized with isoflurane (Baxter) and decapitated. The brain was removed from the skull and chilled for 1 min in cooled (4 °C) artificial cerebrospinal fluid (ACSF) containing 125 mM NaCl, 2.6 mM KCl, 1.4 mM $MgSO_4$, 2.5 mM $CaCl_2$, 1.1 mM $NaH_2PO_4$, 27.5 mM $NaHCO_3$ and 11.1 mM D-glucose, pH 7.2, 310 mOsm/kg. The hippocampus was transversally cut in 400 µm slices (VT1200S, Leica). Slices were equilibrated in a custom-made submerged chamber in ACSF continuously gassed with carbogen (95% O2, 5% CO2) for 30 min at 32 °C and subsequently kept at room temperature.

**Extracellular field recordings.** To avoid recurrent excitation, Schaffer collaterals were severed between CA3 and CA1. We evoked synaptic responses by stimulating the Schaffer collaterals at 0.03–0.1 Hz with 0.2 ms pulses. Field EPSPs (fEPSPs) were recorded in the stratum radiatum of the CA1 region with glass microelectrodes (Science Products) filled with ACSF. Data were acquired using a Multiclamp 700B amplifier (Axon Supplement Instruments), digitized on a Digidata 1440A (Axon Instruments) and stored on a PC. fEPSP slopes were used as a measure of dendritic activity and determined between 20% and 80% of the maximum field amplitude. fEPSP slopes acquired over 2 min were averaged.

**mEPSC recordings.** Miniature EPSCs were recorded in a voltage clamp at –70 mV in ACSF perfusion (125 mM NaCl, 2.6 mM KCl, 1.4 mM $MgSO_4$, 4 mM $CaCl_2$, 2.7 mM $MgCl_2$, 1.1 mM $NaH_2PO_4$, 27.5 mM $NaHCO_3$ and 11.1 mM D-glucose) supplemented with tetrodotoxin (0.2 µM), picrotoxin (100 µM) and trichlormethiazide (250 µM) to increase mEPSC frequency. Recording electrodes had a resistance of 3–5 MΩ pulled from borosilicate glass (Science Products). Internal solution contained 150mM CsGluconate, 8 mM NaCl, 2 mM MgATP, 10 mM HEPES, 0.2 mM EGTA, and 5 mM QX-314 ([2-[(2,6-dimethylphenyl)amino]-2-oxoethyl]-triethylazanium bromide), pH 7.2, 290 mOsm/kg. mEPSCs were detected off-line and statistically analyzed with a custom-written Matlab routine (MathWorks).

**Immunoblotting experiments.** For immunoblotting, cells and tissue were lysed in RIPA buffer containing protease inhibitors (Roche), 20 µM *N*-ethylmaleimide (NEM) and 1,10-orthophenathroline (OPT) (Sigma-Aldrich). Protein samples were separated by 8–14% SDS-PAGE and transferred to 0.45 µm polyvinylidene difluoride membranes (Millipore). Membranes were then incubated with the respective primary and secondary horseradish peroxidase–conjugated antibodies. Chemiluminescence signals were acquired in a ChemiDoc station and analyzed with Image Lab (Bio-Rad). Developed X-ray films were scanned and quantified with ImageJ.

**Immunoprecipitation experiments.** Cells were lysed in RIPA buffer or NP-40 buffer containing protease inhibitors (Roche), 20 µM NEM and 1,10-OPT (Sigma-Aldrich). Protein lysates were briefly precleared with Dynabeads Protein G (Invitrogen) and then incubated with the respective antibody or antibody-conjugated magnetic beads. For nonconjugated antibodies, the antibody-protein complexes were precipitated with Dynabeads Protein G. Immunoprecipitated proteins bound to beads were washed with buffer containing 10 mM Tris, pH 7.4, 1 mM EDTA, pH 8.0, 1 mM EGTA, pH 8.0, 150 mM NaCl, 0.1–0.5% Triton X-100 and protease inhibitors. For immunoprecipitation under denatured conditions, cells were lysed in 6 M GmCl buffer (6 M guanidinium-HCl, 10 mM Tris-HCl, 0.1 M $Na_2HPO_4/NaH_2PO_4$, pH 8.0, 10 mM β-mercaptoethanol). For immunoprecipitation of 6xHis-tagged proteins, 15 mM imidazole (Sigma-Aldrich) was added to the lysis buffer. Lysates were incubated with magnetic Streptavidin beads (Pierce) or nickel–nitrilotriacetic acid beads (Qiagen). Beads were successively washed once with 6 M GmCl buffer containing 0.1% Triton X-100, once with 8 M urea buffer, pH 8.0 (8 M urea, 0.1 M $Na_2HPO_4/NaH_2PO_4$, 0.01 M Tris-HCl, 10 mM β-mercaptoethanol and 0.1% Triton X-100), and three times with 8 M urea buffer, pH 6.3. Proteins were eluted by boiling in 4× Laemmli buffer, separated by SDS-PAGE and analyzed by immunoblotting. 6xHis-tagged proteins were eluted with 200 mM imidazole.

**Brain fractionation.** The preparation of synaptosomes, synaptic vesicles, plasma membranes and postsynaptic densities of hippocampi or forebrains of C57BL/6 mice was performed as previously described[65,66]. All procedures were performed at 4 °C; all buffers and reagents included complete protease inhibitor cocktail (Roche), phosphatase inhibitor cocktails I and II (Sigma-Aldrich) plus 5 mM sodium orthovanadate, 20 µM NEM and 1,10-OPT. Postsynaptic densities were further purified from the synaptic plasma membrane fraction according to Cho *et al.*[65]. Samples were lysed in SDS-containing buffer and subjected to immunoblotting.

**Mass spectrometry.** The immunopurified proteins were separated by SDS-PAGE, and PSD-95 bands at ~100 and ~130 kDa were cut and subjected to in-gel tryptic digestion. Peptides were analyzed using liquid chromatography–electrospray ionization–tandem mass spectrometry, and Nedd8- and ubiquitin-modified lysine residues were identified using the Mascot search engine.

**Protein identification and ubiquitylation/neddylation localization.** Prior to the protein database search, the tandem mass spectrometry spectra were converted to mzData format using a conversion tool embedded in Bioworks software (version 3.1, Thermo Scientific). The protein database searches were performed using the Mascot engine (http://www.matrixscience.com). Mass spectra were searched against the Swiss-Prot 15.3 database (uniprot29.05.09), choosing *Rattus norvegicus* for primary rat neurons and *Mus musculus* for primary mouse neurons, and with transfected heterologous HEK cells as the taxonomy

specimen. The peptide and the fragment mass accuracies were set to 20 ppm and 0.6 Da, respectively. Full tryptic peptides including one missed cleavage were accepted. Carboxyamidomethylation at cysteine was set as a static modification. Methionine oxidation; serine, tyrosine and threonine phosphorylation; and lysine modification by GG and LRGG tags were set as variable modifications. The GG-tag modification ($m/z$ 114) of lysine residues results from trypsin cleavage of ubiquitin or Nedd8; the LRGG tag ($m/z$ 383) results specifically from ubiquitin in the case of a missed cleavage. For the Nedd8 mutants, AGG ($m/z$ 185) or LGG ($m/z$ 227) modification tags were added to the list of variable modifications. With mass spectrometry, typically 10–15% of all theoretical tryptic peptides of a protein are identified[67]. To enhance the protein sequence coverage, we repeated the database search using 'SemiTrypsin' as the enzyme. The semitryptic peptides include more than 90% of nontryptic peptides generated during trypsin digestion[68]. The Mascot database search was performed with a confidence index > 95% and with thresholds for the peptide score and the expected peptide score of >20 and <19, respectively. The mass spectra of GG-, LRGG-, AGG- and LGG-modified peptides were confirmed by manual inspection.

**Behavior.** All experiments were performed with male mice. Behavioral testing took place in the first half of the animals' light period, except for the water-cross maze and fear conditioning paradigms, in which the animals were tested during the dark period. The water-cross maze, used to assess spatial learning, was performed as previously described[69]. Spatial memory was investigated with the Y-maze with an intertrial interval (ITI) of 30 min as described previously[70]. Object recognition memory (30 min ITI) was investigated in the Y-maze. Long-term object-recognition memory (24 h ITI) was assessed in an open-field apparatus. In the first trial animals were allowed to freely explore two identical simple-shaped objects. After the ITI, one of the familiar objects was replaced by a novel one. The sociability and social novelty/memory tests were performed with a three-chamber apparatus as previously described[71]. Contextual and auditory fear memory were assessed as previously described[53,72]. The dark-light box, elevated plus-maze, elevated zero maze and novelty-induced hypophagia tests were used to assess anxiety-related behavior as previously decribed[53].

**Frequency-domain-based FRET–fluorescence-lifetime imaging measurements of the FRET pair PSD-95::GFP/γ-2::mCherry.** Experiments were performed as previously described[34]. Acquisitions and fluorescence intensity analysis were carried out with MetaMorph software (Molecular Devices).

**Fluorescence recovery after photobleaching microscopy.** The FRAP experiments were performed as previously described[73]. Diffraction-limited regions expressing PSD-95::GFP were photobleached for 5 ms with a 491 nm laser. Recovery from photobleaching was monitored with 224 consecutive acquisitions in time-lapse mode, a prebleach sequence of 11 frames at 2 images/s, a postbleach sequence of 100 frames at 10 images/s, a sequence of 60 frames at 2 images/s and finally a sequence of 53 frames at 0.2 images/s. The images were corrected for background noise and continuous photobleaching using the MetaMorph software. Recovery curves were normalized to the fluorescence measured before the bleach, and residual fluorescence right after the bleach was set to zero.

**Statistical analysis.** Each data set shown was obtained from at least three independent experiments. Data distribution was assumed to be normal, but this was not formally tested. No statistical methods were used to predetermine sample sizes, but our sample sizes are similar to those reported in previous publications[22,53,61,62]. Animals were assigned to the various experimental groups on the basis of genotype. Age-matched littermates were used as controls in all experiments. No animals were excluded from analyses. No randomization was used. For immunofluorescence and animal experiments, data collection and analysis were performed blinded to the conditions of the experiment. Statistical analysis was carried out using GraphPad Prism 5 software (GraphPad Software), SigmaPlot 12.5 and Microsoft Excel. Data are presented as mean ± s.e.m. and box-and-whisker minimum-maximum plots. Statistical significance was assessed via two-tailed unpaired Student's $t$ test, one-way ANOVA or two-way ANOVA followed by Bonferroni's post hoc comparisons when appropriate. Correlation was assessed using Pearson's correlation coefficient ($r$). mEPSC amplitude and frequency/interevent interval were assessed using the Kolmogorov-Smirnov test (Matlab). Differences were considered statistically significant at $^{*}P < 0.05$ and $^{**}P < 0.01$.

A **Supplementary Methods Checklist** is available.


51. Shirogane, T., Jin, J.P., Ang, X.L. & Harper, J.W. SCF beta-TRCP controls Clock-dependent transcription via casein kinase 1-dependent degradation of the mammalian Period-1 (Per1) protein. *J. Biol. Chem.* **280**, 26863–26872 (2005).
52. Kamura, T., Conrad, M.N., Yan, Q., Conaway, R.C. & Conaway, J.W. The Rbx1 subunit of SCF and VHL E3 ubiquitin ligase activates Rub1 modification of cullins Cdc53 and Cul2. *Genes Dev.* **13**, 2928–2933 (1999).
53. Refojo, D. *et al.* Glutamatergic and dopaminergic neurons mediate anxiogenic and anxiolytic effects of CRHR1. *Science* **333**, 1903–1907 (2011).
54. Dymecki, S.M. Flp recombinase promotes site-specific DNA recombination in embryonic stem cells and transgenic mice. *Proc. Natl. Acad. Sci. USA* **93**, 6191–6196 (1996).
55. Erdmann, G., Schütz, G. & Berger, S. Inducible gene inactivation in neurons of the adult mouse forebrain. *BMC Neurosci.* **8**, 63 (2007).
56. Feng, G.P. *et al.* Imaging neuronal subsets in transgenic mice expressing multiple spectral variants of GFP. *Neuron* **28**, 41–51 (2000).
57. Kühne, C. *et al.* Visualizing corticotropin-releasing hormone receptor type 1 expression and neuronal connectivities in the mouse using a novel multifunctional allele. *J. Comp. Neurol.* **520**, 3150–3180 (2012).
58. Dotti, C.G., Sullivan, C.A. & Banker, G.A. The establishment of polarity by hippocampal neurons in culture. *J. Neurosci.* **8**, 1454–1468 (1988).
59. Allen, J.W., Mutkus, L.A. & Aschner, M. Isolation of neonatal rat cortical astrocytes for primary cultures. *Curr. Protoc. Toxicol.* **Chapter 12** Unit 12.4 (2000).
60. Harris, K.M. & Kater, S.B. Dendritic spines—cellular specializations imparting both stability and flexibility to synaptic function. *Annu. Rev. Neurosci.* **17**, 341–371 (1994).
61. Sala, C. *et al.* Regulation of dendritic spine morphology and synaptic function by Shank and Homer. *Neuron* **31**, 115–130 (2001).
62. Okamura, K. *et al.* Cadherin activity is required for activity-induced spine remodeling. *J. Cell Biol.* **167**, 961–972 (2004).
63. Saito, T. *In vivo* electroporation in the embryonic mouse central nervous system. *Nat. Protoc.* **1**, 1552–1558 (2006).
64. Stoppini, L., Buchs, P.A. & Muller, D. A simple method for organotypic cultures of nervous tissue. *J. Neurosci. Methods* **37**, 173–182 (1991).
65. Cho, K.O., Hunt, C.A. & Kennedy, M.B. The rat-brain postsynaptic density fraction contains a homolog of the *Drosophila* disks-large tumor suppressor protein. *Neuron* **9**, 929–942 (1992).
66. Blackstone, C.D. *et al.* Biochemical characterization and localization of a non-N-methyl-D-aspartate glutamate receptor in rat brain. *J. Neurochem.* **58**, 1118–1126 (1992).
67. States, D.J. *et al.* Challenges in deriving high-confidence protein identifications from data gathered by a HUPO plasma proteome collaborative study. *Nat. Biotechnol.* **24**, 333–338 (2006).
68. Alves, P. *et al.* Fast and accurate identification of semi-tryptic peptides in shotgun proteomics. *Bioinformatics* **24**, 102–109 (2008).
69. Kleinknecht, K.R. *et al.* Hippocampus-dependent place learning enables spatial flexibility in C57BL6/N mice. *Front. Behav. Neurosci.* **6**, 87 (2012).
70. Wang, X.D. *et al.* Forebrain CRF1 modulates early-life stress-programmed cognitive deficits. *J. Neurosci.* **31**, 13625–13634 (2011).
71. Hartmann, J. *et al.* Fkbp52 heterozygosity alters behavioral, endocrine and neurogenetic parameters under basal and chronic stress conditions in mice. *Psychoneuroendocrinology* **37**, 2009–2021 (2012).
72. Kamprath, K. & Wotjak, C.T. Nonassociative learning processes determine expression and extinction of conditioned fear in mice. *Learn. Mem.* **11**, 770–786 (2004).
73. Petrini, E.M. *et al.* Endocytic trafficking and recycling maintain a pool of mobile surface AMPA receptors required for synaptic potentiation. *Neuron* **63**, 92–105 (2009).





doi:10.1038/nn.3912